Bull Earthquake Eng (2015) 13:3151–3186
DOI 10.1007/s10518-015-9756-8

ORIGINAL RESEARCH PAPER

Diagonal cracking shear strength of unreinforced masonry panels: a correction proposal of the *b* shape factor

Michele Betti[1] · Luciano Galano[1] · Michele Petracchi[2] · Andrea Vignoli[1]

Received: 24 March 2014 / Accepted: 31 March 2015 / Published online: 21 April 2015

Abstract After summarising the failure criteria adopted by the new Italian Seismic Code (NTC 2008) for the seismic assessment of unreinforced masonry panels (URM), the paper presents a numerical study aimed at investigating the *b* shape factor. This factor is a coefficient, function of the panels' slenderness, employed to evaluate the ultimate shear strength of URM for the failure mechanism with diagonal cracking. The results herein presented show that the actual values of the coefficient *b* are higher than those proposed by the NTC (2008); consequently, the shear strength obtained by applying the Italian Seismic Code is not conservative. An amendment is proposed for the *b* shape factor, and its effects are evaluated through the analysis of three plane-URM walls with regular openings and different slenderness of the masonry beams. Pushover analyses were performed to estimate their seismic capacity and their collapse modes. The walls were modelled by both the finite element method (FEM) and the equivalent frame approach (EFM). In the EFM approach the *b* shape factor was selected both according to the NTC (2008) and as proposed in the paper. The seismic capacity curves show that the EFM approach significantly overestimate the ultimate shear strength of the walls with respect to the results obtained by the FEM, and this effect is amplified when the *b* shape factor is evaluated as recommended by the NTC (2008).

✉ Michele Betti
mbetti@dicea.unifi.it

Luciano Galano
luciano@dicea.unifi.it

Michele Petracchi
michele.petracchi@gmail.com

Andrea Vignoli
avignoli@dicea.unifi.it

[1] Department of Civil and Environmental Engineering (DICeA), University of Florence, Via di Santa Marta, 3, 50139 Florence, Italy

[2] Viale Palmiro Togliatti, 143, 50019 Sesto Fiorentino, FI, Italy

Keywords Unreinforced masonry panels · Shear failure · Diagonal cracking · b Shape factor · Plane masonry walls

List of main symbols

b	Shape factor associated to the shear stress distribution in the central horizontal section of the masonry panel
c	Cohesion
d_{cu}	Maximum displacement of the control point
e	Axial load eccentricity
η	Dilatancy angle
E	Longitudinal modulus of elasticity
φ	Friction angle
f_d	Design compressive strength of the masonry
f_{td}	Design tensile strength of the masonry
f_{vd}	Design shear strength of the masonry for sliding
f_{vd0}	Ultimate design shear strength of masonry without compression
f_{hd}	Ultimate design compressive strength of the masonry in the horizontal direction
f_{vk0}	Characteristic shear strength for sliding without axial force on the panel section
f_t	Tensile strength of the masonry
G	Shear modulus of elasticity
γ_M	Partial safety factor
h	Height of vertical section of the spandrel or height of the pier
K_e	Initial stiffness
l	Panel width
l'	Length of the compressive portion of the transversal section of the masonry panel
λ	Slenderness of masonry panels ($\lambda = h/l$)
M	Acting bending moment
M_u	Ultimate bending moment
v	Poisson's ratio
P	Actual compressive axial load
σ_0	Average normal stress acting on the whole masonry panel section [$\sigma_0 = P/(lt)$]
σ_n	The same as σ_0 calculated as $\sigma_n = P/(l't)$, being l' less than l
t	Wall thickness
τ_{0d}	The same as f_{vk0} considering the shear failure with diagonal cracking
τ_k	Characteristic shear strength of the masonry
τ_u	Ultimate average shear stress
V_t	Ultimate shear strength
V_p	Shear strength required for the equilibrium of a beam subject to M_u
V_b	Base shear
V_{bu}	Maximum base shear
w	Weight per unit volume

1 Introduction

In 2008 the Italian Ministry of Public Works issued the new Seismic Code for buildings and infrastructures (NTC 2008; Circular 2009). These technical Recommendations introduced significant changes for the assessment of existing buildings and for the design of

new ones in seismic areas. Main revisions, for masonry constructions, concerned both the methods of structural analysis and the criteria to be adopted to verify the masonry walls under seismic loads.

For a masonry wall subjected to in-plane seismic loads the previous Italian Recommendations (DM 1996; Circular 1981) assumed two collapse typologies. The first failure mode was adopted for masonry walls with very stiff and strong spandrels (Fig. 1a). In this case, it was assumed that walls collapse for shear failure of the masonry piers. The second failure mode was employed for walls with slender spandrels and, in this case, it was assumed that walls collapse for combined shear and bending loads of the masonry spandrels (Fig. 1b). According to a common interpretation the first calculus scheme was associated with short walls such as those of buildings with few stories (two or three stories); equally, the second scheme was associated with slender walls such as those of multi-storey buildings (four or more stories). As a result, the slenderness of the piers was habitually confused with the slenderness of the walls, whereas it is evident that the panels' slenderness depends on the dimensions of the neighbouring openings rather than the overall slenderness of the wall (Augenti 2004). In addition, the Circular (1981) adopted the Turnšek and Cacovic shear failure criterion (Turnšek and Cacovic 1971) to verify each masonry panel under in-plane seismic loads. This criterion assumes that a masonry pier fails for shear, developing a main diagonal crack starting from the centre of the panel. Some examples of application were also reported in the Appendix of the Circular (1981) were the calculus steps were detailed for masonry buildings with regular openings. According to the scheme of Fig. 1a, the same employed for the so-called shear-type frame structures, each floor of the building was analysed separately from the other floors, and for each masonry pier a shear collapse mode with diagonal cracking was assumed. The POR method (Tomaževic 1978) was one of the most common tools used to implement this calculus. Hence, as highlighted by Augenti (2004), many structural designers, and the public authorities, were convinced that the POR method had general validity so it was applied for the seismic verification of all masonry buildings, regardless of the effective failure mode of each masonry panel.

The current Italian technical Recommendations (Technical standards for constructions, NTC 2008) have partially removed these ambiguities since they assume both shear and flexure collapse modes for masonry panels, and require that the structural analysis of a construction must be carried out for the entire building, to satisfy the global balance equations. This is specifically requested for the design of new buildings, even if the NTC 2008 still allows the use of the POR method for the assessment of structural masonry units

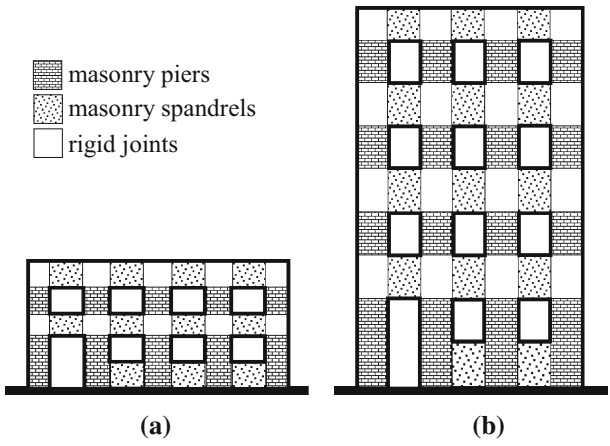

Fig. 1 Models of masonry walls according to the Circular (1981); **a** buildings with 2 or 3 stories, **b** buildings with 4 or more stories

(SU) of aggregation buildings (i.e. adjacent and/or interconnected structures having an unitary behaviour from a static and seismic point of view). This is underlined at point 8.7.1 of the Recommendations, where it is reported that: "*the verification of a structural unit with stiff enough floors can be performed, even for buildings with more than two floors, by static nonlinear analysis, analysing and verifying each level separately, and neglecting the variation of the axial force in masonry panels due to the effect of the seismic loads*". However, even in these cases, as the specific failure criteria to be adopted are not indicated, it is understood that the masonry piers and beams may collapse for shear with diagonal cracking or for combined flexure and axial loads, depending on their slenderness.

Within this general context, the paper deepens the diagonal cracking shear failure criterion for unreinforced masonry panels (URM) as assumed by the NTC (2008), and is organised as follows: in Sect. 2, a review of the failure modes of masonry panels (piers and spandrels) proposed by the Italian Code is briefly sketched, together with a comparison with other international Standards. The criticisms of the shear strength criterion with diagonal cracking, which are motivations of the research, are explained in Sect. 3 where the effects of the b shape factor are discussed. In Sect. 4 it is shown that the b factor, here evaluated by linear and nonlinear finite element (FE) analyses, assumes values that significantly differ from those adopted in Circular (2009). According to the numerical results, an amendment for the b shape factor as function of the panel slenderness is proposed in Sect. 5. Eventually, in Sect. 6, the effects of the proposed formulation are evaluated analysing the seismic behaviour of three plane masonry walls, characterised by different slenderness of the masonry panels, and comparing the results among different numerical approaches.

2 Failure modes of masonry panels

The behaviour of masonry elements under in-plane loads (shear walls) depends on several factors, among which: the materials, the boundary conditions, the precompression level and the aspect ratio. Different combinations of these variables can lead to different failure modes. The observation of the damages induced by past seismic events to masonry buildings, together with laboratory experimental investigations, showed that masonry panels subjected to in-plane loads have two basic typologies of behaviour (Calderini et al. 2009; FEMA 306 1998): I) Failure by flexure. Two different types of failure for flexure may occur, depending on the precompression level. If the applied vertical load is low, the horizontal load produces tensile flexural cracking at the corners, and the panel begins to behave as a nearly rigid body rotating about the toe (rocking). If, due to a high applied vertical load, no significant flexural cracking occurs, the panel is progressively characterised by a widespread damage pattern, with sub-vertical cracks oriented towards the more compressed corners (crushing). II) Failure by shear. A first shear failure mode is the shear sliding failure, where the collapse is characterised by sliding on a horizontal bed joint, usually located at one of the end section of the masonry panel. The second failure mode occurs with diagonal cracking where the collapse is reached with the formation of a diagonal crack, which develops from the centre of the panel and subsequently propagates towards the corners. This failure mode may be activated when the principal tensile stresses developed in the centre of the panel exceed the tensile strength of masonry, due to a combination of vertical and horizontal loads.

Many interactions may occur between the above mentioned collapse mechanisms, hence it is not always simple to recognise the occurrence of a specific failure mode. In the

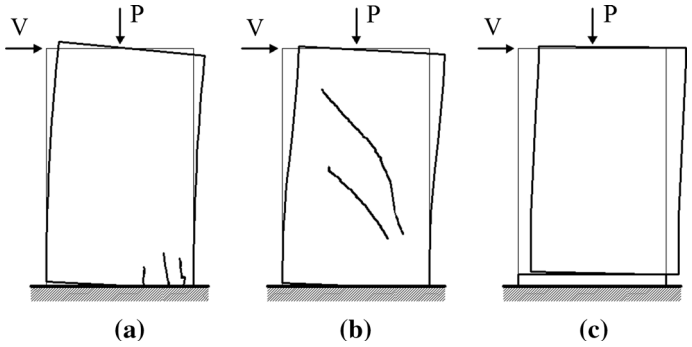

Fig. 2 In-plane failure modes of masonry piers subjected to shear: **a** flexural; **b** shear with diagonal cracking; **c** shear sliding

past, many experimental researches have attempted to assess the influence of the relevant parameters (boundary conditions, precompression level, aspect ratio, masonry texture, etc.) on the failure mode of masonry panels. As a general remark, it is possible to observe that the flexural failure mode (rocking mechanism) prevails when there are low compression load levels or high aspect ratios; rocking tends to prevail in slender piers. For increasing levels of vertical compression, diagonal cracking prevails over rocking in moderately slender piers, while bed joint sliding occurs only in very squat piers. Furthermore, diagonal cracking is typically more relevant for panels with double-bending boundary conditions since the response is mainly dominated by the shear behaviour (Magenes and Calvi 1997; Calderini et al. 2009; FEMA 306 1998).

Among the above reported collapse mechanisms, the Italian Seismic Code (NTC 2008; Circular 2009) considers the following three different failure modes for URM panels (Fig. 2), distinguishing between masonry piers and masonry beams (spandrels): (a) flexural failure under combined axial load and bending moment, (b) shear failure with diagonal cracking and (c) shear sliding failure. Accordingly, the Code provides the proper equations for evaluating the ultimate design strengths as next summarised.

2.1 Strength of masonry piers

For masonry piers, the design flexural strength, expressed in terms of ultimate bending moment, is given by:

$$M_u = \frac{Pl}{2}\left(1 - \frac{\sigma_0}{0.85 f_d}\right) \tag{1}$$

The ultimate shear strength for the diagonal cracking collapse mode is defined through Eq. (2):

$$V_t = lt\frac{f_{td}}{b}\sqrt{1 + \frac{\sigma_0}{f_{td}}} = lt\frac{1.5\tau_{0d}}{b}\sqrt{1 + \frac{\sigma_0}{1.5\tau_{0d}}} \tag{2}$$

Strictly Eq. (2) is proposed for the assessment of existing buildings, but is also useful for the design of new structures.

The ultimate shear sliding strength is given by Eq. (3):

$$V_t = l' t f_{vd} = l' t \frac{f_{vk0} + 0.4\sigma_n}{\gamma_M} = l' t \frac{\left(f_{vk0} + 0.4\frac{P}{l't}\right)}{\gamma_M} \tag{3}$$

Symbols corresponding to the geometrical items in Eqs. from (1) to (3) denote: l is the panel width, t is the wall thickness and b is a shape factor (the shear stress distribution factor) associated to the shear stress distribution in the central cross horizontal section of the panel. Symbols corresponding to the mechanical items denote: f_d is the design compressive strength of the masonry, f_{td} is the design tensile strength of the masonry, f_{vd} is the design shear strength for sliding, f_{vk0} is the characteristic shear strength for sliding without axial force on the panel cross-section and τ_{0d} is the same as f_{vk0} considering the shear failure with diagonal cracking. The coefficient γ_M is a partial safety factor. Finally, P is the compressive axial load, σ_0 is the average normal stress acting on the whole section of the masonry panel [$\sigma_0 = P/(lt)$] and σ_n is the same as σ_0 calculated as $\sigma_n = P/(l't)$ being $l' < l$; l' is the length of the compressed portion of the section, and it may be evaluated as follows:

$$l' = 3\left(\frac{l}{2} - e\right) = 3\left(\frac{l}{2} - \frac{M}{P}\right) \tag{4}$$

in which e denotes the axial load eccentricity and M is the actual bending moment ($l' = 0$ if $e > l/2$).

Analysing Eq. (2) it is possible to observe that, according to the Circular (2009), the characteristic shear strength τ_{0d} and the tensile strength f_{td} of the masonry are associated by the following relation:

$$f_{td} = 1.5\tau_{0d} \tag{5}$$

Hence, according the NTC (2008), the strength τ_{0d} loses its original meaning of masonry shear strength without compressive stress, unless b is equal to 1.5. Actually, τ_{0d} is a purely mechanical characteristic associated to f_{td} adopted to define the ultimate shear V_t.

2.2 Strength of masonry beams (spandrels)

Previous Eqs. from (1) to (3) can be also employed for the design of masonry beams if the axial load P on the spandrels is known.

On the contrary, if the axial load is unknown (as in those cases where the numerical analyses are performed with shear-type equivalent frame models with the assumption of floor diaphragms perfectly rigid in-plane), the ultimate bending moment is given by:

$$M_u = \frac{H_p h}{2}\left(1 - \frac{H_p}{0.85 f_{hd} h t}\right) \tag{6}$$

whereas the ultimate shear strength is defined as the lowest value between Eqs. (7) and (8):

$$V_p = \frac{2M_u}{l} \tag{7}$$

$$V_t = ht\, f_{vd0} \tag{8}$$

V_p is the shear strength required for the equilibrium of the beam subject to M_u, and V_t is the ultimate shear sliding strength. Symbols corresponding to the geometrical items in Eqs. from (6) to (8) denote: h is the height of the vertical section of the masonry beam, t is the wall thickness and l is the span of the beam. Symbols corresponding to the mechanical

items are: f_{vd0} is the ultimate design shear strength of masonry without compression, f_{hd} is the ultimate design compressive strength of masonry in the horizontal direction and H_p is the lowest value between the tensile strength of a tie passing across the beam (if existing) and the quantity $0.4 f_{hd}\ ht$. The technical Rules NTC (2008) and Circular (2009), allow the use of Eqs. (6), (7) and (8) only if the masonry beam is reinforced with a horizontal tie passing across the spandrel like a steel rod or a reinforced concrete (RC) beam. The tensile force developed by the tie is, in fact, essential to equilibrate the compressive force acting on the beam section at the opposite side. For URM beams the only proper shear failure criterion, even though not expressly specified, is the one with diagonal cracking. So, the ultimate shear may be evaluated through Eq. (2) with h instead of l (if σ_0 is unknown it may be supposed equal to zero).

Besides, the NTC (2008) introduced a significant difference between the design of new buildings and the assessment/rehabilitation of existing constructions. In the first case, the design strengths of the masonry are evaluated applying specific safety factors to the characteristic strength values. In the second case, the design strengths are evaluated applying the same safety factors but to the average values.

It is worth noting that the NTC (2008) is one of the few Codes that explicitly provide different expressions for the evaluation of the shear strength of masonry panels distinguishing between failure modes with diagonal cracking and joint sliding. The majority of Codes assumes a Mohr–Coulomb-type verification criterion without explicitly declare the failure mode. This is the case, for instance, of the Eurocode 6 (EN 1996-1 2005). Recently Tomaževic (2009), discussing the results of a series of laboratory tests, shows that in case of shear diagonal cracking failure, the provisions of the Eurocode 6 are not in agreement with the actual resistance of masonry walls, highlighting that the shear failure mechanism with diagonal cracking is predominant. On the contrary, FEMA 306 (1998) and FEMA 356 (2000) clearly distinguish between the two shear failure modes and, in case of shear failure with diagonal cracking, they adopt an expression similar to those assumed by the Italian Rules. In particular, the FEMA 306 (1998) incorporate an equation for evaluating the diagonal shear strength V_{dt} of URM panels subjected to in-plane shear forces according to Turnšek and Sheppard (1980):

$$V_{dt} = f'_{dt} A_n (\beta) \sqrt{1 + \frac{f_{ae}}{f'_{dt}}} \tag{9}$$

where f'_{dt} denote the diagonal tension strength, A_n the area of net grouted section, f_{ae} the vertical axial compressive stress and, finally, β is a coefficient (reciprocal to the b shape factor of the Italian Code) equal to 0.67 for $L/h_{eff} < 0.67$, L/h_{eff} when $0.67 \geq L/h_{eff} \leq 1.0$, and 1.0 when $L/h_{eff} > 1$ with h_{eff} the height to resultant of lateral force, and L the length of wall or pier. This expression was also maintained by the FEMA 356 (2000) [Eq. (10)], but with modified applicable L/h_{eff} limits:

$$Q_{CL} = f'_{dt} A_n \left(\frac{L}{h_{eff}}\right) \sqrt{1 + \frac{f_a}{f'_{dt}}} \tag{10}$$

where A_n, h_{eff} and L, are the same as given for previous equation.

Turnšek and Sheppard (1980) and FEMA 306 (1998) [Eq. (9)] capped L/h_{eff} at 1.0, but there was no upper limit on this ratio in FEMA 356 (2000), hence the shear strength evaluated according Eq. (10) could be increased according to the wall aspect ratio (Tremayne et al. 2012). The term L/h_{eff} was introduced in FEMA 356 (2000) with the aim to improve

correlation with experimental results, but several authors (Chen et al. 2008) pointed out the need of further investigation on its actual expression. The new ASCE/SEI 41-06 (2006) does not include diagonal cracking as a failure mechanism, but considering that this is a relevant observed collapse mode in buildings subjected to earthquakes, a subcommittee determined that it should be reintroduced into the 2013 ASCE provisions. As discussed by Tremayne et al. (2012), the ASCE 41-13 will consider for the evaluation of diagonal cracking strength the same equation included in FEMA 306 (1998), maintaining the upper limit of 1.0 on L/h_{eff}. The debate on this point highlighted the need of further investigation to cover the existing gaps in the current understanding of URM shear diagonal cracking criteria.

3 The *b* shape factor of the shear diagonal cracking failure criterion

The previous Italian Standards, the one issued in 1996 (DM 1996), adopted Eq. (11) to evaluate the shear strength of a masonry panel (implicitly assuming a shear failure mode with diagonal cracking):

$$V_t = lt\,\tau_k\sqrt{1+\frac{\sigma_0}{1.5\tau_k}} \tag{11}$$

in which τ_k is the so-called characteristic shear strength of the material (without compressive stresses), depending on the masonry typology. Equation (11) was originally provided in the Appendix of the technical document of 30 July 1981 (Circular 1981) and it was the only failure criterion proposed to evaluate the shear strength of a masonry panel and verify masonry buildings under seismic loading. Equation (11) was used within a nonlinear method of structural analysis (the POR method) and was originally proposed by Turnšek and Cacovic for masonry panels subjected to shear and compression under double bending constraint conditions (Turnšek and Cacovic 1971). They assumed that the first crack appears at the centre of the panel when the positive principal tensile stress reaches the tensile strength f_t of the masonry. Then the cracks propagate along the diagonal of the panel up to collapse (Fig. 2b). Given the brittleness of the masonry, this condition can be approximately considered concurrent with the failure of the panel. If $f_t = 1.5\tau_k$ is assumed, then Eq. (11) holds. It is worth noting that Eq. (11) is satisfactory only for panels in which the values of the slenderness ratio $\lambda = h/l$ are in agreement with the de Saint–Venant's hypotheses. In fact, the quantity $1.5\tau_k$ represents the maximum shear stress at the centre of a panel with rectangular section only in case the de Saint–Venant's hypotheses regarding the slenderness ratio are met.

If τ_{0d} is assumed the same as τ_k, and $f_t = f_{td}$, Eqs. (2) and (11) are equal only if $b = 1.5$. The Circular (2009) connect f_{td} and τ_{0d} by Eq. (5) hence, the parameter τ_{0d} loses the original meaning of masonry pure shear strength except when $b = 1.5$. However, at point C8.7.1.5, b is defined as a function of the slenderness λ of the panels, adopting the original formulation of Benedetti and Tomaževic (1984). Explicitly: "*b is a corrective coefficient that takes into account the variability of the shear stresses along the central cross-section, depending on the panel slenderness. It is proper to assume b = h/l, but no more than 1.5 nor less than 1.0, being h the height of the panel*". Hence:

$$b = \begin{cases} 1.0\ldots\ldots & for \quad \lambda = h/l \le 1.0 \\ \lambda\ldots\ldots & for \quad 1.0 < \lambda = h/l < 1.5 \\ 1.5\ldots\ldots & for \quad 1.5 \le \lambda = h/l \end{cases} \tag{12}$$

Table 1 *b* Shape factor values

Panel	λ	*b* Eq. (12), from (Circular 2009)	*b* Eq. (13), from (Chiostrini and Vignoli 1994)	Difference (%)
T1	1	1.00	1.37	+37
T2	1	1.00	1.40	+40
T3	1	1.00	1.29	+29
T4	1	1.00	1.19	+19
COR1	1	1.00	1.23	+23
COR2	1	1.00	1.33	+33
Ist. Belm.	1	1.00	1.14	+14

The *b* shape factors according to Turnšek and Cacovic (1971) and Benedetti and Tomaževic (1984) are compared in Fig. 6.

Despite its simplicity for practical use, Eq. (12) is not fully proper since the shear strength obtained by adopting Eq. (2) is overestimated for panels with slenderness ratios lower than 1.5. This can be shown analysing some of the results of previous researches, as next reported.

Chiostrini and Vignoli (1994) evaluated the mechanical characteristics of masonry panels with unitary slenderness ratio ($\lambda = h/l = 1$) by means of in situ tests through a shear-compression setup. They calculated the *b* factor by applying the formula of Turnšek and Sheppard (1980):

$$(\lambda = 1) \quad b = 1.543 - 0.478\frac{\tau_u}{\sigma_0} \tag{13}$$

where τ_u denotes the ultimate average shear stress. Table 1 resumes the *b* values obtained by the authors applying Eq. (13) to their experimental results. In the same table such values are compared with those obtained by Eq. (12) of Benedetti and Tomaževic. The percentage differences are significant.

Calderini et al. (2009) carried out nonlinear FE analyses of three masonry panels with increasing slenderness ratio: $\lambda = 0.65$ for panel Pier-1, $\lambda = 1.35$ for panel Pier-2 and $\lambda = 2.00$ for panel Pier-3. The three panels were subjected to a constant axial load and to an increasing horizontal displacement applied at the top section, under double bending constraint conditions. The panels Pier-1 and Pier-2 collapsed for shear with diagonal cracking, whereas Pier-3 collapsed for flexure (rocking). Analysing the numerical results for each panel, it is evident that the *b* shape factor changes as a function of stresses and deformations. In the elastic range the average values for *b* obtained by the numerical analyses were: 1.33 for Pier-1 ($\lambda = 0.65$), 1.44 for Pier-2 ($\lambda = 1.35$) and 1.48 for Pier-3 ($\lambda = 2.00$). The corresponding values near collapse were: 1.15 for Pier-1, 1.37 for Pier-2 and 1.50 for Pier-3. Hence, it is clear that for Pier-1 and Pier-2 the *b* factor has values significantly dissimilar from those provided by Eq. (12), also in the nonlinear range. The authors agree with these conclusions and observe that for Pier-1 ($\lambda = 0.65$) the *b* shape factor is never less than 1.15.

Therefore the results of the analysed researches show that the effective values of the *b* shape factor are appreciably different from those suggested by the Circular (2009), especially for short panels ($\lambda \leq 1$) or panels with medium slenderness ratio ($1 < \lambda < 1.5$).

4 Numerical investigations on the *b* shape factor

The above results highlight the need to deepen the relationship between the b shape factor and the panel slenderness λ. This relationship was herein analysed by performing first linear and next nonlinear analyses on masonry panels with variable slenderness and evaluating the shape factor as the ratio between the maximum and the average shear stress in the central cross-section of each panel. A comprehensive study should also evaluate the influence of the boundary conditions (i.e. limit cases of double bending and single bending), the influence of the mechanical properties of the masonry (i.e. elastic modulus, Poisson's ratio, masonry strength) and the effect of the vertical compressive stresses acting on the panel. The numerical investigations herein presented do not consider all of the above factors, being primarily focused on the relationship between b and the panel slenderness λ. Nevertheless, in the authors' opinion, these analyses provide effective information to assess the variability of the factor b.

4.1 Linear analysis

A first set of numerical analyses was performed investigating the linear elastic range of behaviour. This assumption agrees with the Turnšek and Cacovic hypothesis of the shear failure criterion with diagonal cracking (i.e. "the stress state is evaluated by assuming masonry as an elastic, homogeneous and isotropic material, until the beginning of the first crack"; Turnšek and Cacovic 1971). Two-dimensional isoparametric finite elements with 4 nodes were employed, and 67 different masonry panel geometries (variable aspect ratio) in double bending boundary conditions were analysed (Fig. 3). The nodes at the base of the models were fixed both in the x (horizontal) and z (vertical) direction, while the nodes at the top section of the panels were constrained in the z direction and free in the x direction. The adopted mechanical properties of the masonry are reported in Table 2.

The analyses denoted by A ($\nu = 0$, $E/G = 2$), although not fully relevant to real cases, aim to analyse the function $b(\lambda)$ in this limit condition. The parameters used in the analyses denoted by B ($\nu = 0.5$, $E/G = 3$) are very close to those of a real stone masonry walls (and were selected according to the masonry typologies as defined in the Circular 2009).

Overall, 134 cases were analysed (67 with material parameters A and 67 with material parameters B). The height of the panels was updated to obtain varying slenderness between

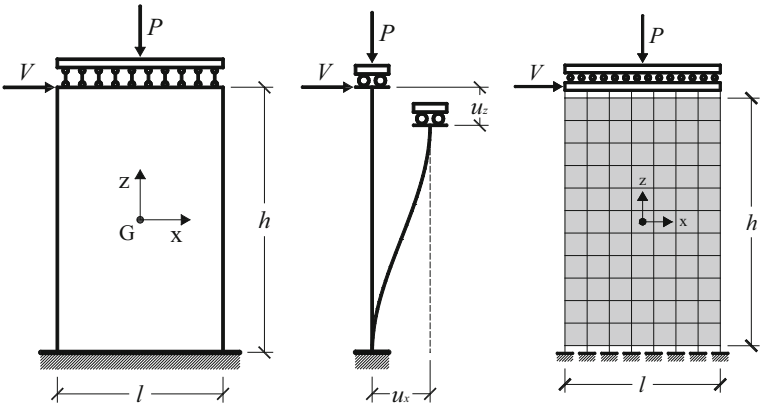

Fig. 3 Masonry piers subjected to shear (V) and compression (P) with double bending boundary conditions

Table 2 Mechanical properties of masonry used in the linear FEM analyses

	E (N/mm^2)	G (N/mm^2)	v
Case A	2000	1000	0.00
Case B	2000	667	0.50

0.015 and 3.0, whereas the width and the thickness of each panel were fixed equal to 1000 mm. The panels were meshed with square finite elements whose dimensions were modified according to the actual geometry. Panels were first subjected to a compressive load P of 1 N, and subsequently a shear force V of 1 N was applied on the top section. The b shape factor is defined as the ratio between the maximum shear stress $\tau_{zx,max}$ and the average shear stress $\tau_{zx,av}$ (shear stresses are evaluated at the central cross-section of the panels) through Eq. (14):

$$b = \frac{\tau_{zx,\max}}{\tau_{zx,av}} = \frac{\tau_{zx,\max}}{V}\, lt \tag{14}$$

Results of the numerical analyses were also used to evaluate the distribution of τ_{zx} along the central cross-section of the panels as function of their slenderness. Figure 4 shows this distribution for panels A, while Fig. 5 shows the same distribution for panels B. The plots are presented in dimensionless form and refer to 12 different values of slenderness (λ ranging from 0.015 up to 1.526). They show that when $\lambda \leq 1$ the distribution of the shear stresses τ_{zx} is not uniform along the cross-section; only in the cases where λ is very small (0.015–0.053) τ_{zx} tends asymptotically to such a condition. Hence, in the panels with $\lambda \leq 1$ the shape factor cannot be assumed equal to 1.0. Figure 6 compares the function $b(\lambda)$ obtained by Eq. (14) with the proposal of Turnšek and Cacovic ($b = 1.5$) and the formula suggested by Benedetti and Tomaževic (1984). It is evident that for panels with $\lambda < 1.5$ the values of the b factor obtained by the numerical analyses still differ appreciably from those obtained by Eq. (12) adopted in the Circular (2009). For panels with $\lambda > 1.5$ (when the slenderness ratio λ is in agreement with the de Saint–Venant's hypothesis) the b factor tends asymptotically to the straight line $b = 1.5$. The functions $b(\lambda)$ shown in Fig. 6 are also reported in Table 3 for selected slenderness values (where it is possible to observe that, as expected, the Poisson's ratio has a very limited effect on the calculated b shape factor).

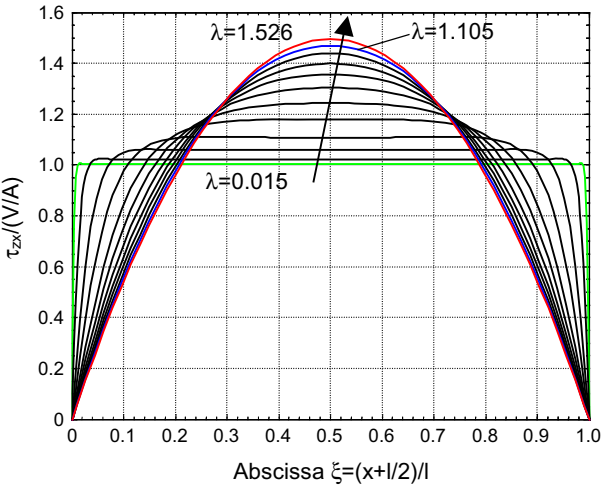

Fig. 4 Shear stresses τ_{zx} in the central cross-section of panels (linear FE analyses, case A)

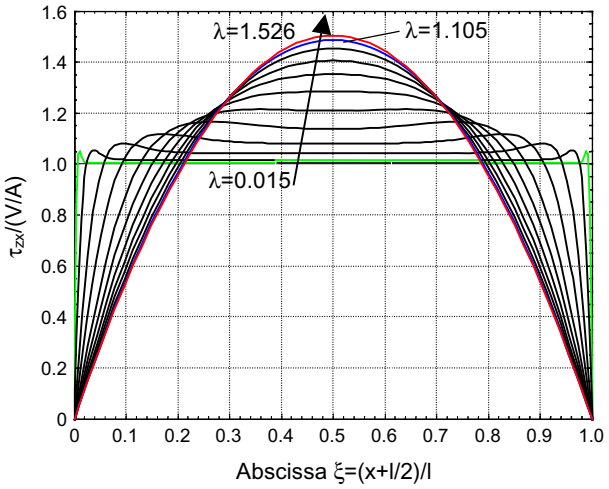

Fig. 5 Shear stresses τ_{zx} in the central cross-section of panels (linear FE analyses, case B)

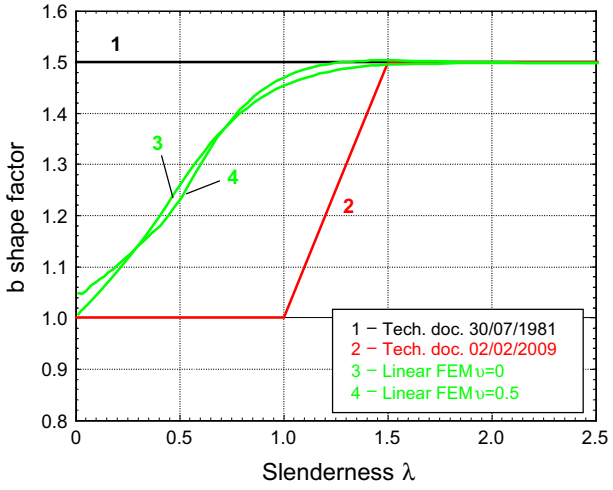

Fig. 6 Comparisons of the *b* shape factor evaluated according to the previous Italian Standard (Circular 1981), the actual Italian Standard (Circular 2009) and the results of the linear FE analyses

Results illustrate that the distribution of the shear stress in the central cross-section of a masonry panel subject to shear load does not differ from the one predicted by the de Saint–Venant's model, even if the slenderness decreases. The distribution of the shear stress τ_{zx} differs from the uniform one ($b = 1$) already for very small slenderness (0.015–0.053). In the actual load-bearing masonry structures it is rather unusual to find panels with slenderness less than 0.3, therefore, it is evident that the condition $b = 1$ is very rare, and consequently Eq. (12) is not reliable for short panels.

4.2 Nonlinear analysis

A second group of tests was carried out analysing the masonry panels beyond the linear elastic field. To this aim the general purpose code ANSYS (1992) was employed, and three-dimensional isoparametric finite elements with 8 nodes (*solid 65*) were adopted to

Table 3 *b* Shape factor versus panel slenderness (linear analyses)

Slenderness λ	Case A	Case B
0.015	1.01	1.05
0.028	1.01	1.05
0.040	1.02	1.05
0.053	1.02	1.05
0.095	1.04	1.07
0.137	1.06	1.08
0.200	1.09	1.10
0.242	1.11	1.12
0.298	1.14	1.14
0.333	1.16	1.15
0.404	1.20	1.18
0.509	1.26	1.24
0.614	1.32	1.31
0.719	1.37	1.37
0.860	1.42	1.43
0.930	1.44	1.45
1.000	1.45	1.47
1.105	1.47	1.49
1.211	1.48	1.50
1.316	1.49	1.50
1.491	1.49	1.50
2.053	1.50	1.50
2.579	1.50	1.50
3.000	1.50	1.50

model the masonry panels. Mechanical nonlinearities were reproduced by combining the Drucker–Prager plasticity criterion (DP) (Drucker and Prager 1952) with the Willam–Warnke concrete failure criterion (WW) (Willam and Warnke 1975).

The material parameters required to define the DP model, the cohesion c and the internal angle of friction φ, are introduced in such a way that the circular cone yield surface of the DP model corresponds to the outer vertex of the hexagonal Mohr–Coulomb yield surface. The DP yield surface can be written as follows (Drucker and Prager 1952):

$$F = \alpha I_1 + \sqrt{J_2} - k = 0 \tag{15}$$

where I_1 is the first invariant of the Cauchy stress and J_2 denotes the second invariant of the deviatoric part of the Cauchy stress. The two parameters α and k, required to define the yield DP surface, are connected with the cohesion c and the friction angle φ by the following equations:

$$\alpha = \frac{2 \sin \varphi}{\sqrt{3}(3 - \sin \varphi)}; \quad k = \frac{6c \cos \varphi}{\sqrt{3}(3 - \sin \varphi)} \tag{16}$$

The two parameters α and k allow to evaluate the yield stresses in uniaxial tension and compression, respectively f_{tDP} and f_{cDP}, by:

$$f_{tDP} = \frac{k}{\frac{1}{\sqrt{3}} + \alpha}; \quad f_{cDP} = \frac{k}{\frac{1}{\sqrt{3}} - \alpha} \tag{17}$$

Cohesion c and the angle of internal friction φ were then assumed as the only two material parameters to define the yield surface.

The WW failure criterion, originally proposed for concrete (Willam and Warnke 1975), accounts for both cracking and crushing failure modes through a smeared model. The criterion is defined by the following inequality:

$$\frac{F}{f_C} - S \leq 0 \tag{18}$$

where F is a function of the principal stress state (Willam and Warnke 1975), S is a failure surface expressed in terms of principal stresses and f_c is the uniaxial crushing strength. If Eq. (18) is satisfied, cracking or crushing are not expected. Otherwise the material will crack or crush.

The crisis criteria of masonry, cracking in tension and crushing in compression, were reproduced through the proper intersection of the two surfaces. To calibrate the parameters, the uniaxial tensile strength of the concrete model (f_{tWW}) must be assumed smaller than the correspondent value of the plastic domain (f_{tDP}) to reproduce the actual masonry cracking in tension. In addition, to reproduce the correct plastic behaviour of the masonry in the mixed compression-traction zones, the compression of the concrete model (f_{cWW}) must be selected greater than the strength (f_{cDP}) of the open curve of the Drucker-Prager model. As a result, the material behaves as an isotropic medium with plastic deformation, cracking and crushing capabilities. Both the DP and WW criteria are frequently employed in the inherent literature to model the mechanical behaviour of masonry structures. Among the others, Zucchini and Lourenço (2007) adopt, discussing the homogenisation approach for masonry, the DP model for the simulation of the plastic deformation in masonry cells. They show how it is possible by using the DP criterion to account for the degradation of the mechanical properties of masonry in compression. Chiostrini et al. (1998) combine the DP criterion with the WW failure surface to model, through a macro-element approach, the results of several diagonal tests on masonry samples obtaining good agreement with the experimental results. The DP criterion combined with the WW model has been recently adopted in a whole masonry structure by Betti et al. (2014) to discuss the seismic behaviour of URM buildings with flexible diaphragms through the investigation of a reference masonry prototype tested on shaking table at the CNR-ENEA research centre of Casaccia (Roma, Italy). Comparison between numerical and experimental results showed the effectiveness of the approach.

The constitutive parameters here employed for the DP criterion and the WW failure domain are reported in Table 4; these parameters were calibrated according to the masonry typologies defined in the Circular (2009). It is worth mentioning, lastly, the difference of the tensile and compressive strengths of the DP criterion ($f_{tDP} = 0.216$ N/mm^2, $f_{cDP} = 1.522$ N/mm^2) and those of the WW failure criterion ($f_{tWW} = 0.15$ N/mm^2, $f_{cWW} = 4.0$ N/mm^2). The combination of these parameters allows an elastic-brittle behaviour in case of biaxial tensile stresses or biaxial tensile-compressive stresses with low compression level. On the contrary, the material is elastoplastic in case of biaxial compressive stresses or biaxial tensile-compressive stresses with high compression level (Betti et al. 2009; Betti and Vignoli 2011).

Table 4 Mechanical properties of the masonry (FEM analyses)

Elastic parameters		
E	Longitudinal modulus of elasticity	2000 N/mm^2
G	Shear modulus of elasticity	800 N/mm^2
v	Poisson's ratio	0.25
w	Weight per unit volume	18.0 kN/m^3
DP criterion parameters		
c	Cohesion	0.24 N/mm^2
φ	Friction angle	55°
η	Dilatancy angle	55°
f_{cDP}	Compressive strength	1.522 N/mm^2
f_{tDP}	Tensile strength	0.216 N/mm^2
WW criterion parameters		
f_{cWW}	Compressive strength	4.00 N/mm^2
f_{tWW}	Tensile strength	0.15 N/mm^2
β_c	Shear stress coefficient (closed cracks)	0.75
β_t	Shear stress coefficient (open cracks)	0.25

With the nonlinear model, 23 distinct geometries of masonry panels were analysed. These panels have the following geometrical dimensions: width $l = 1000$ mm, thickness $t = 200$ mm and height increasing from 300 mm up to 2500 mm with step of 100 mm. The analysed slenderness hence ranges from 0.3 up to 2.5, with increments $\Delta\lambda$ equal to 0.1. The analyses were carried out using the same boundary conditions of double bending adopted in the linear analyses (Fig. 3). Preliminary tests aimed at investigating mesh-dependence were performed, and mesh sizes varying between 50 and 10 mm (with increasing step-size of 5 mm) were considered. Stability of results was analysed checking both stability of distribution and extent of the cracking/crushing pattern and stability of shear stresses distribution along the cross section of a selected number of panels (height $h = 500$, 1000, 1500 and 2000 mm). In all the analysed cases, results have not shown significant mesh-dependence and a mesh size of 20 mm was employed as a compromise between computational costs and discretization accuracy.

Each geometric model was used to perform four types of analysis (for a total of 92 cases):

- LCA 0.4: nonlinear static analysis (under force control), with compression level about 40 % the compressive strength ($P = 0.4ltf_d$).
- DCA 0.4: nonlinear static analysis (under displacement control), with compression level equal to about 40 % of the compressive strength ($P = 0.4ltf_d$).
- LCA 0.6: nonlinear static analysis (under force control), with compression level equal to about 60 % of the compressive strength ($P = 0.6ltf_d$).
- DCA 0.6: nonlinear static analysis (under displacement control), with compression level equal to about 60 % of the compressive strength ($P = 0.6ltf_d$).

The selected compressive levels are rather high if compared to those of the real buildings. Nevertheless this choice was necessary to allow shear (rather than flexural) failures. Moreover, the assumption of medium to high compression vertical stresses is consistent with the hypothesis of double bending boundary condition, which typically occurs in the panels at the lower floors of multi-storey masonry buildings.

Each analysis was carried out in two steps: in the first step the compressive load P was applied at the upper section of the panels, subsequently a shear load V (LCA), or an horizontal displacement u_x (DCA), was applied. The horizontal loading (shear force or displacement) was monotonically applied up to the panel's collapse. It is noteworthy to specify that the nonlinear system of equations was solved by an incremental Newton–Raphson method and consequently the numerical collapse of the panel corresponds to the maximum load that the panel can withstand before the load–deflection capacity curve starts a negative slope (i.e. the load step where the overall stiffness matrix becomes singular). More advanced methods, such as the arc-length method, can be employed for passing limit points during structural calculation but these methods were not used, as it is not required to follow the descending branch of the load–deflection capacity curve.

Numerical results were hence employed to evaluate the shear stresses distribution in the central cross-section of the panels as a function of the dimensionless abscissa ξ varying the slenderness. Figures 7, 8, 9 and 10 show these diagrams, where the shear stresses are in dimensionless form with respect to $\tau_{zx,\ av} = V/A$. The first figure (left) of each pair always refers to the first step of the horizontal loading process (when the panels are still in the linear elastic field), the second figure (right) refers to a step near to the panel (numerical) collapse.

Results allow a few comments. As long as the horizontal load (or displacement) applied at the upper section of the panels does not produce significant cracking and crushing, the distribution of the shear stresses τ_{zx} does not differ from that one obtained with the linear analyses. Again, even for short panels ($\lambda \leq 1.0$) the τ_{zx} have a trend significantly different from the uniform distribution considered by Eq. (12). If λ is close to one the shape of the stresses τ_{zx} is almost parabolic. After the first crack or crush occurs, the shapes of τ_{zx} differ one to each other as a consequence of the spread of the tensile cracking.

Figures 11, 12, 13 and 14 show the collapse cracking pattern with respect to four different slenderness ($\lambda = 0.5$, $\lambda = 1.0$, $\lambda = 1.5$ and $\lambda = 2.0$). The pattern and extent of damage differs, depending both on the slenderness and on the compressive level. The panels with low slenderness ($\lambda = 0.5$) reach collapse presenting a double systems of diagonal cracks in eccentric position. This behaviour is more evident for the two LCA analyses. Panels with high levels of compression (LCA 0.6 and DCA 0.6, see Figs. 11c, d,14c, d) show a crack pattern that covers the whole base and top sections, which probably correspond to sliding shear cracks. The panels with medium slenderness ($\lambda = 1.0$, Fig. 12 and $\lambda = 1.5$, Fig. 13) show the typical shear collapse mode with a system of diagonal cracks. In the case DCA 0.4

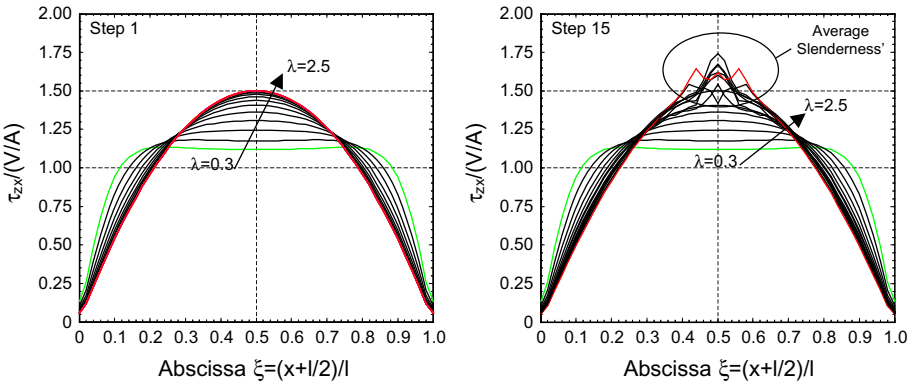

Fig. 7 Shear stresses τ_{zx} in the central cross-section of panels (nonlinear FE analyses, case LCA 0.4; *left*: step 1 and *right*: step 15)

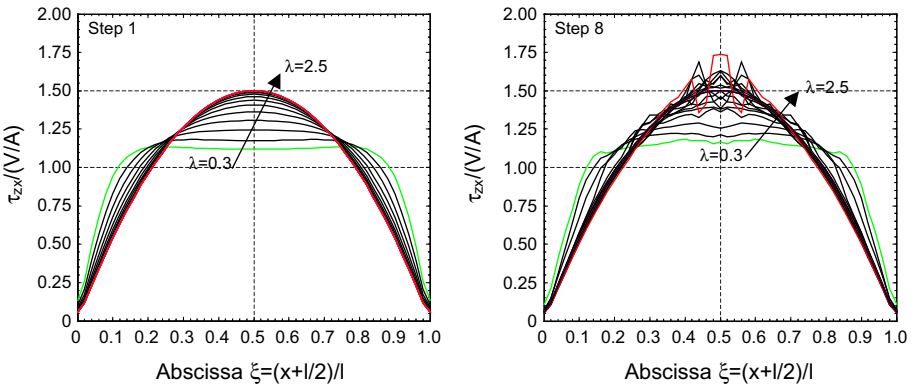

Fig. 8 Shear stresses τ_{zx} in the central cross-section of panels (nonlinear FE analyses, case DCA 0.4; *left*: step 1 and *right*: step 8)

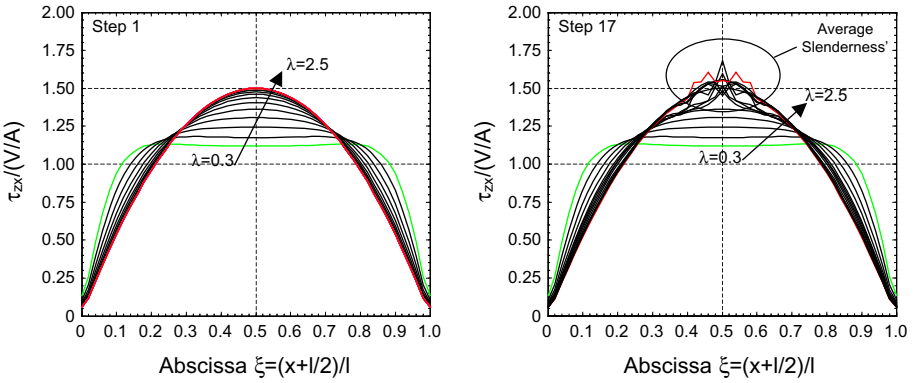

Fig. 9 Shear stresses τ_{zx} in the central cross-section of panels (nonlinear FE analyses, case LCA 0.6; *left*: step 1 and *right*: step 17)

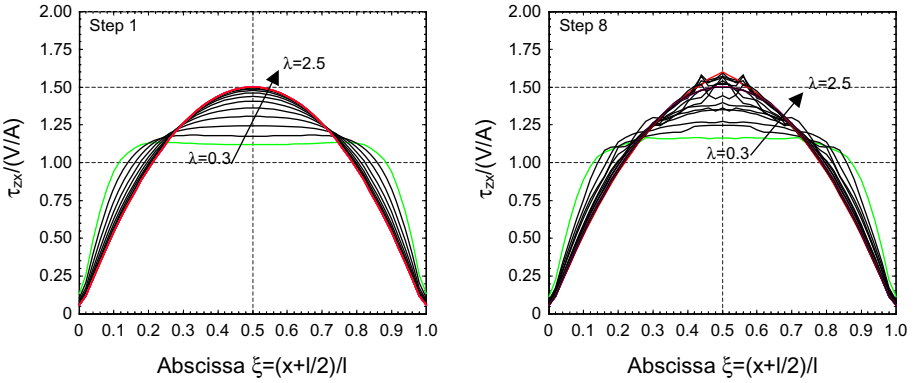

Fig. 10 Shear stresses τ_{zx} in the central cross-section of panels (nonlinear FE analyses, case DCA 0.6; *left*: step 1 and *right*: step 8)

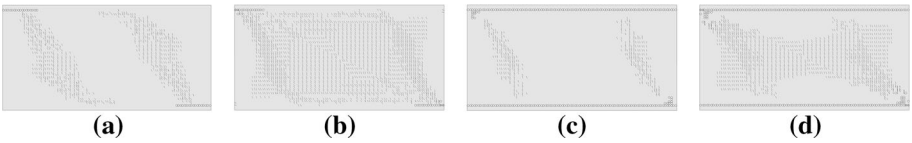

Fig. 11 Collapse cracking patterns of panels with slenderness $\lambda = 0.5$: **a** LCA 0.4; **b** DCA 0.4; **c** LCA 0.6; **d** DCA 0.6

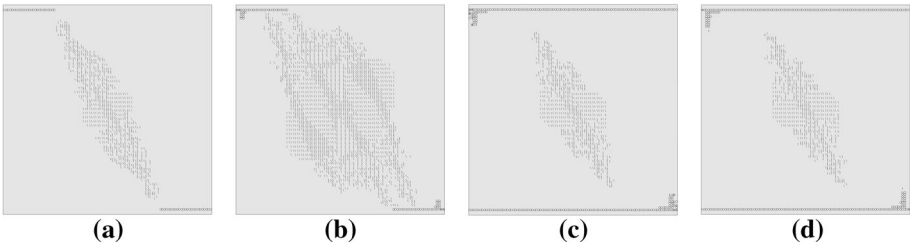

Fig. 12 Collapse cracking patterns of panels with slenderness $\lambda = 1.0$: **a** LCA 0.4; **b** DCA 0.4; **c** LCA 0.6; **d** DCA 0.6

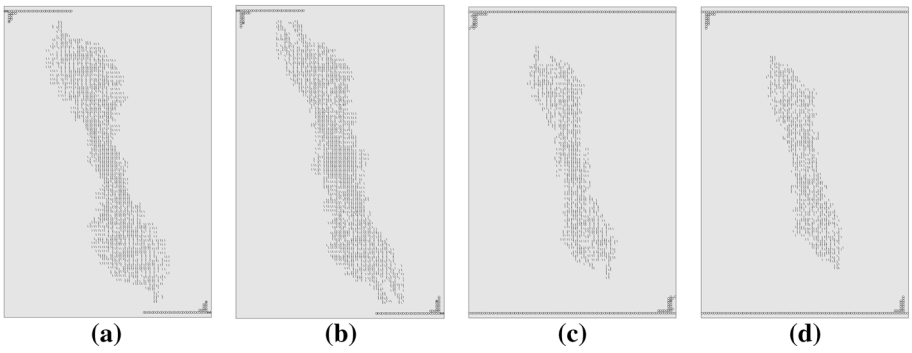

Fig. 13 Collapse cracking patterns of panels with slenderness $\lambda = 1.5$: **a** LCA 0.4; **b** DCA 0.4; **c** LCA 0.6; **d** DCA 0.6

with $\lambda = 1.0$ (Fig. 12b) the crack pattern is larger in width than in the other cases. In the analyses LCA 0.6 (Figs. 11c, 12c, 13c, 14c) and DCA 0.6 (Figs. 11d, 12d, 13d, 14d) a system of cracks appeared along the bottom and top sections of the panel. In the latter two cases is also visible a crushing at the corners. The panels with high slenderness ($\lambda = 2.0$, Fig. 14) collapses developing a cracking pattern in proximity of the end sections. The damage in the top and bottom sections is well interpreted as a crushing of the edges in compression and a crack opening in the edges in tension. Only the panels DCA 0.4 and DCA 0.6 fail with a shear diagonal cracking characterised by a wider spread of the cracks at the end of the diagonal. It is worth noting that the DCA analyses allow to obtain a few additional equilibrium condition with respect to the corresponding LCA analyses, and it results in the more spread of the diagonal shear cracks before the collapse.

Among all the results, a deepening of the DCA 0.4 analysis for the panels with slenderness equal to 0.5–1.0–1.5–2.0 is reported through the illustration of the stress state in

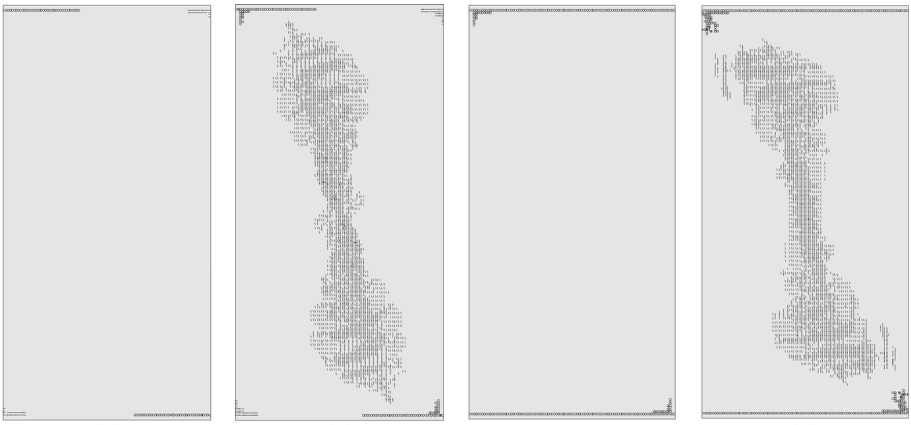

Fig. 14 Collapse cracking patterns of panels with slenderness $\lambda = 2.0$: **a** LCA 0.4; **b** DCA 0.4; **c** LCA 0.6; **d** DCA 0.6

the middle cross-section of the panels (Figs. 15, 16, 17, 18). Concerning the tangential component of the stress it is possible to observe that, in all cases, they start with a parabolic distribution (more evident with the increasing values of slenderness). The distribution of the ratio $\tau_{zx}/\tau_{zx,\,av}$ remains almost parabolic until the panels are in the elastic range, after it is possible to recognise a sudden fall of the stress components. This phenomenon is more evident in panels with slenderness equal to 1.0 and 1.5, and for panels that fails for shear with diagonal cracking. Regarding the normal component of the stress σ_{xx}, this is almost negligible in the first phases of the analyses. With the activation of the nonlinear behaviour, the σ_{xx} progressively passes to compression in all cases and increases until the collapse. This phenomenon can be interpreted as a consequence of the spread of the tensile cracking at the middle cross-sections. This evolution of the normal stresses, which diminishes for increasing values of slenderness, was observed for all the cases and for all the values of the applied axial load.

Linear and nonlinear analyses allowed to evaluate the b shape factor versus slenderness λ and shear V varying the axial load, and such diagrams are reported in Fig. 19 (the values of V are dimensionless with respect to the compressive load P applied to the panels). The surfaces represented in Fig. 19 present a number of irregularities in proximity of the highest level of shear force. They correspond to those steps of the analyses in which, due to nonlinear effects, cracking or crushing occur. As a consequence of the damage the shear stresses lose their regularity and therefore also the b factor loses its smoothness, as indicated by Eq. (14). The surfaces of the four diagrams are smooth until the response of the panels is linear. Nevertheless, beyond a certain excursion in the nonlinear field, the definition of the shape factor loses its meaning due to the irregularity of the distribution of τ_{zx} (a sudden fall occurs in correspondence of the activation of the diagonal cracks and increases as a consequence of the spread of the tensile flexural cracking).

Given the impossibility to identify the b factor beyond a certain amount of damage of the panels it was decided to evaluate the function $b(\lambda)$ just before the arising of the highlighted irregularities. The diagrams $b(\lambda)$ as obtained through the four sets of numerical analyses are shown in Fig. 20 (curve 3) where they are compared with those proposed by Turnšek and Cacovic (curve 1) and Benedetti and Tomaževic [Eq. (12), curve 2]. The four numerical

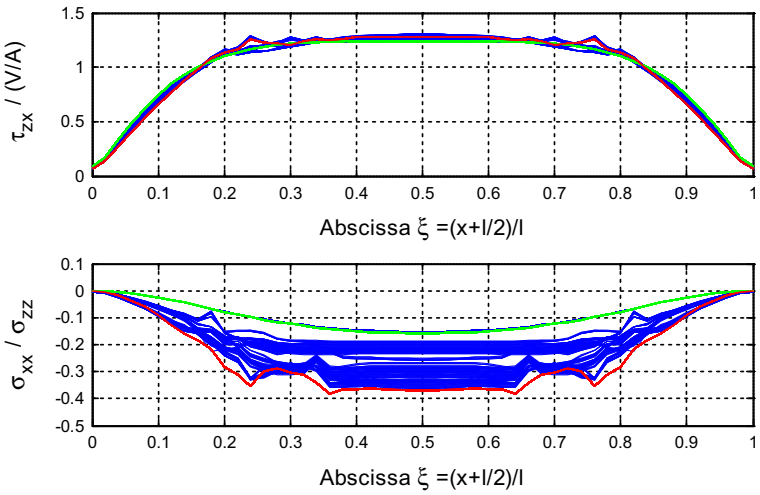

Fig. 15 Shear (*Up*) and normal (*Down*) stress evolution in the central cross-section (DCA 0.4, $\lambda = 0.5$)

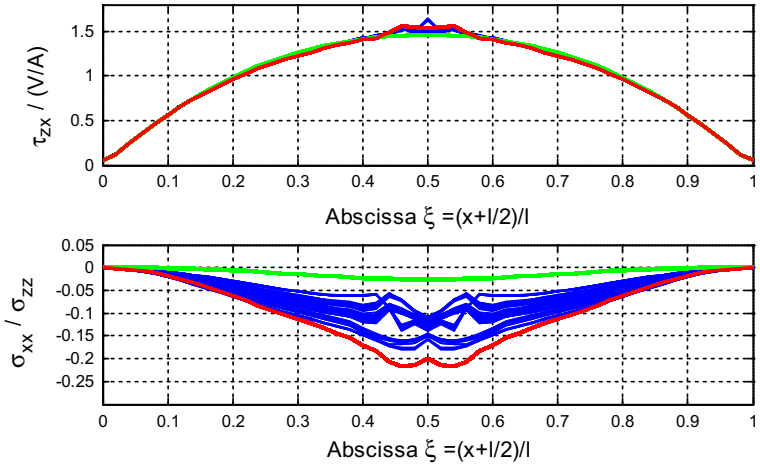

Fig. 16 Shear (*Up*) and normal (*Down*) stress evolution in the central cross-section (DCA 0.4, $\lambda = 1.0$)

curves are coincident indicating that neither the type of analysis (LCA rather than DCA) nor the level of compression produces significant differences. The obtained values for the coefficient b are also reported in Table 5 as average of the four analysed series.

5 The correction proposal for the b(λ) function

The results show that for masonry panels with slenderness λ lower than 1.5 Eq. (12) provides an evident underestimation of the b shape factor, thus producing in turn an overestimation of the shear strength V_t, as defined by Eq. (2).

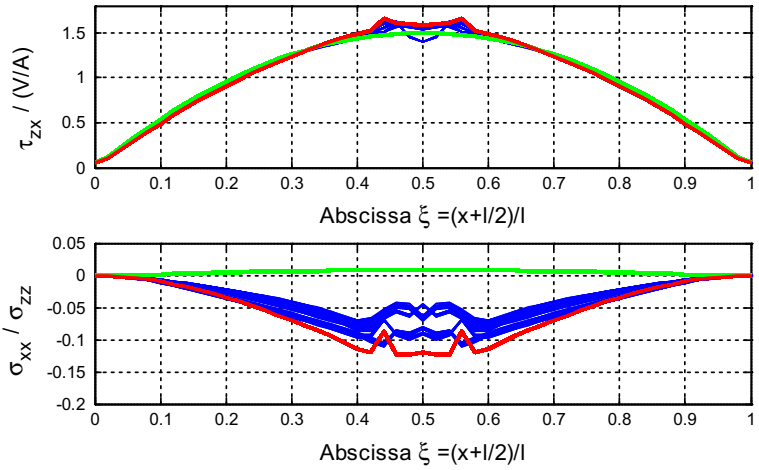

Fig. 17 Shear (*Up*) and normal (*Down*) stress evolution in the central cross-section (DCA 0.4, $\lambda = 1.5$)

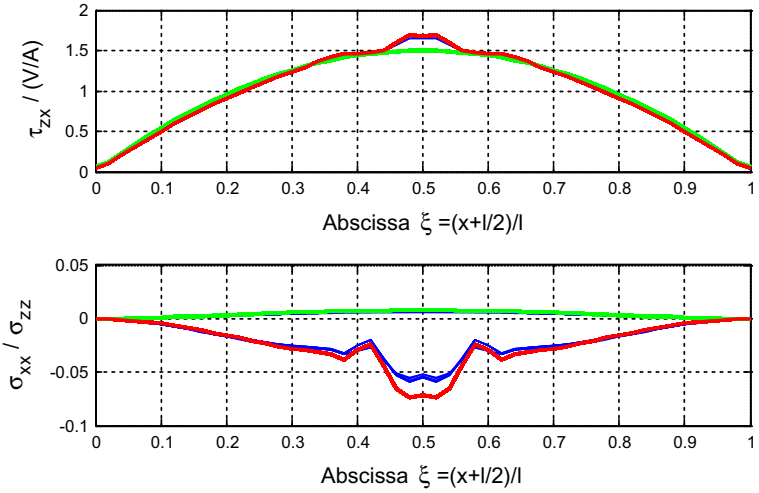

Fig. 18 Shear (*Up*) and normal (*Down*) stress evolution in the central cross-section (DCA 0.4, $\lambda = 2.0$)

This can be demonstrated by plotting the strength domains for masonry panels with slenderness lower than 1.5, and comparing the shear strength predicted by Eq. (2) by using different expressions for the b shape factor. To focus the role of the b factor and the slenderness λ Eq. (2) was rearranged in the following dimensionless form:

$$\frac{V_t}{A\tau_{0d}} = \frac{1.5}{b(\lambda)}\sqrt{1+\frac{2}{3}\left(\frac{\sigma_0}{\tau_{0d}}\right)} \tag{19}$$

The structure of Eq. (19) is not modified by the specific relation existing between the b factor and the slenderness λ, since the shear strength basically depends on the ratio σ_0/τ_{0d} and the slenderness λ of the panels.

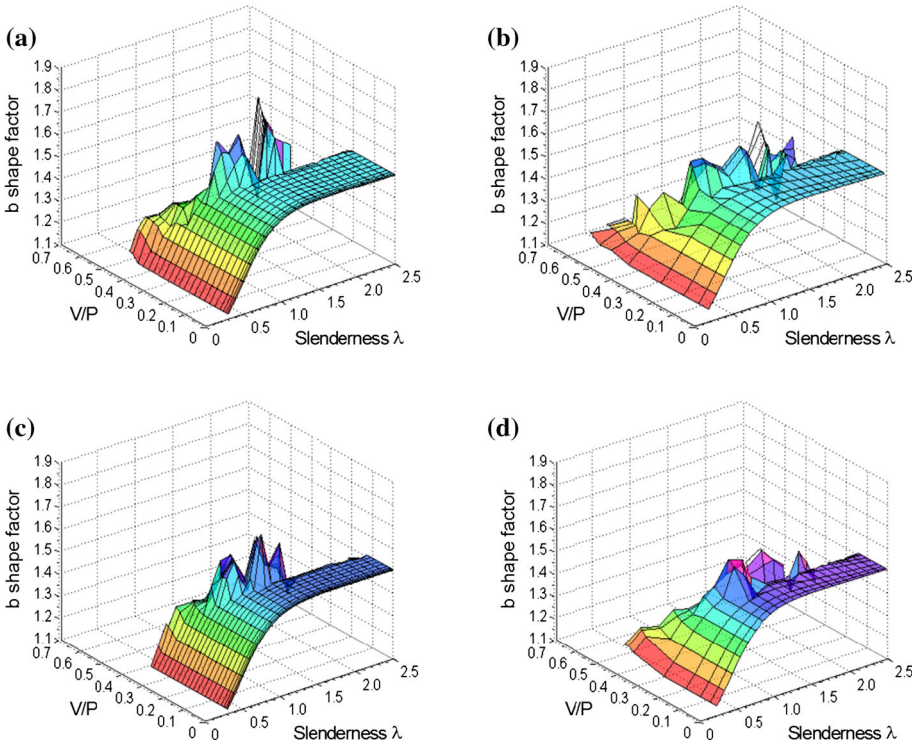

Fig. 19 Variability of the *b* shape factor: **a** analyses LCA 0.4; **b** analyses DCA 0.4; **c** analyses LCA 0.6; **d** analyses DCA 0.6

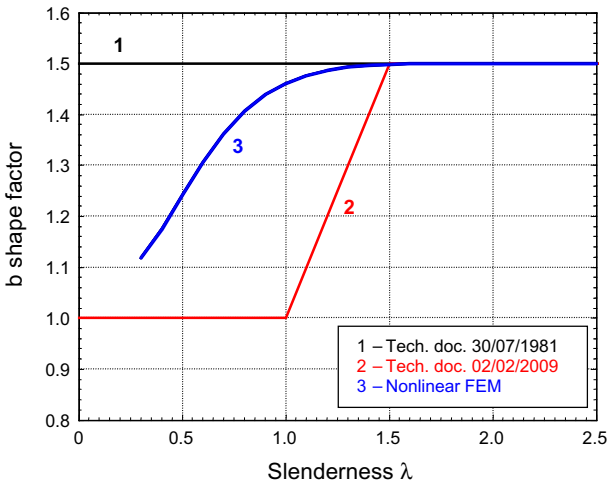

Fig. 20 Comparisons of the *b* shape factor evaluated according to the previous Italian Standard (Circular 1981), the actual Italian Standard (Circular 2009) and the results of the nonlinear FE analyses

As example of panels with λ lower than 1.5, Pier-1 and Pier-2 previously analysed by Calderini et al. (2009) ($\lambda = 0.65$ for Pier-1 and $\lambda = 1.35$ for Pier-2) are considered. Figure 21 shows the shear strength domains for these two panels [Eq. (19)] where the

Table 5 *b* Shape factor versus panel slenderness (nonlinear analyses)

Slenderness λ	*b* (average)
0.3	1.12
0.4	1.18
0.5	1.24
0.6	1.31
0.7	1.36
0.8	1.41
0.9	1.44
1.0	1.46
1.1	1.48
1.2	1.49
1.3	1.49
1.4	1.50
1.5	1.50
1.6	1.50
1.7	1.50
1.8	1.50
1.9	1.50
2.0	1.50
2.1	1.50
2.2	1.50
2.3	1.50
2.4	1.50
2.5	1.50

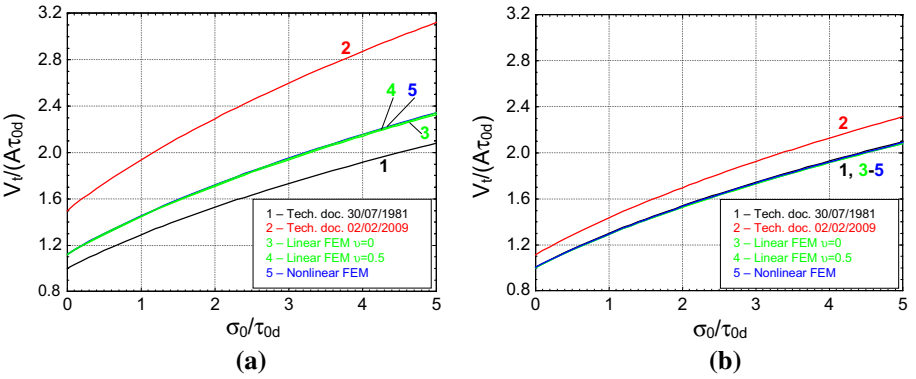

Fig. 21 Comparisons of shear strengths V_t varying the definition of *b*; **a** panel Pier-1 ($\lambda = 0.65$, Calderini et al. 2009), **b** panel Pier-2 ($\lambda = 1.35$, Calderini et al. 2009)

coefficient *b* was evaluated according to: (a) the Turnšek and Cacovic criterion (curve 1), (b) the Benedetti and Tomaževic criterion (curve 2), (c) the results of the linear FE analyses of cases A and B (curves 3 and 4) and (d) the results of the nonlinear FE analyses (curve 5).

The shear strength evaluated with $b = 1$ (Benedetti and Tomaževic criterion) obtained for panel Pier-1 is greater than the others; the greatest difference is obtained when it is compared with the strength evaluated assuming $b = 1.5$ (according to Turnšek and Cacovic criterion). This difference is less evident for panel Pier-2 due to its higher slenderness; yet, the shear strength evaluated assuming b according to the Circular (2009) is still greater than those obtained when b is evaluated according the results of this study or assuming $b = 1.5$ according to Turnšek and Cacovic. For both panels, the shear strengths obtained according to the linear and nonlinear FE analyses are more in agreement with those obtained with the Turnšek and Cacovic criterion than those obtained with the Benedetti and Tomaževic one. Basically results of FE analyses show a significant disagreement with the proposal of b of Eq. (12) as reported in the Circular (2009) that, in addition, overestimates the shear strength.

It is consequently useful to propose an amendment to the actual expression for the b shape factor adopted by the Italian Standards (Circular 2009). The numerical results were hence employed to define an interpolating expression for the b shape factor, as function of the panel slenderness λ. To this aim, the values of b reported in Table 5 were interpolated in the range $0.3 \leq \lambda \leq 1.5$ by using cubic splines. The whole range was divided in six sub-intervals, and in each of them the function $b(\lambda)$ was interpolated through the following third-degree polynomial expression:

$$S_i(\lambda) = A_i\lambda^3 + B_i\lambda^2 + C_i\lambda + D_i \quad i = 1, 2, \ldots, 6 \tag{20}$$

where $i = 1, 2,\ldots,6$ is the subscript that identifies the sub-intervals, and the coefficients A_i, B_i, C_i and D_i vary in each sub-interval. By imposing the continuity of the second derivatives of the polynomials at the beginning and at the end of each sub-interval the following linear system holds:

$$\begin{cases} S_i(\lambda_i) = b(\lambda_i) & for \quad i = 1, 2, \ldots, 6 \\ S_i(\lambda_{i+1}) = b(\lambda_{i+1}) & for \quad i = 1, 2, \ldots, 6 \\ S_i'(\lambda_{i+1}) = S_{i+1}'(\lambda_{i+1}) & for \quad i = 1, 2, \ldots, 5 \\ S_i''(\lambda_{i+1}) = S_{i+1}''(\lambda_{i+1}) & for \quad i = 1, 2, \ldots, 5 \end{cases} \tag{21}$$

where λ_i and λ_{i+1} are the abscissas of the edges of the *i-th* sub-interval. The whole number of unknowns is 24, therefore the 22 equations in (21) must be completed with two additional conditions, i.e.: a) requiring that the second derivative is zero in the left corner of the first sub-interval (natural spline):

$$S_1''(\lambda_1) = 0 \tag{22}$$

and b) imposing the tangency condition at the asymptote $b = 1.5$ at the right corner of the last sub-interval (edge $\lambda_7 = 1.5$):

$$S_6'(\lambda_7) = 0 \tag{23}$$

Table 6 reports the coefficients resulting from the solution of the linear system, and Fig. 22 shows the interpolating function [curve (1)] compared with the original numerical results. The interpolating function matches quite well the numerical results. Nevertheless, an even simpler expression can be proposed for b to approximate the numerical results [Fig. 22, curve (2)]:

$$b(\lambda) = 1.0 + 0.5\lambda, \quad b \leq 1.5 \tag{24}$$

Table 6 Interpolation coefficients for the splines of Eq. (20)

Sub-interval	A_i	B_i	C_i	D_i
$0.3 \leq \lambda < 0.5$	−0.6736	1.0104	0.14267	1.0021
$0.5 \leq \lambda < 0.7$	−1.1798	1.7697	−0.2370	1.0654
$0.7 \leq \lambda < 0.9$	0.4166	−1.5828	2.1098	0.5178
$0.9 \leq \lambda < 1.1$	0.2864	−1.2313	1.7934	0.6127
$1.1 \leq \lambda < 1.3$	0.3812	−1.5441	2.1375	0.4865
$1.3 \leq \lambda < 1.5$	−0.2727	1.0063	−1.1779	1.9232

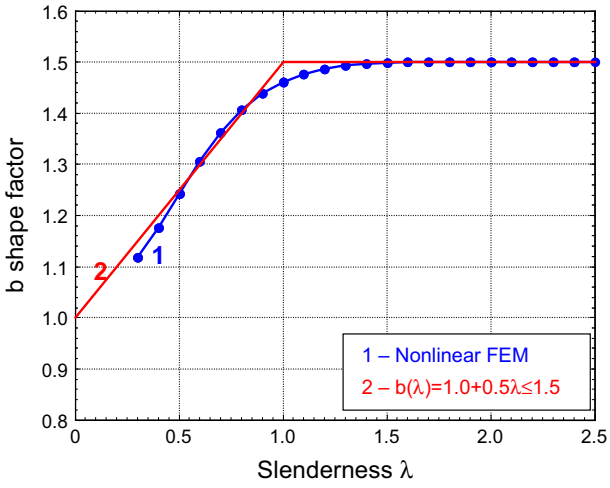

Fig. 22 Diagrams of $b(\lambda)$ obtained by interpolation of the nonlinear FE analyses (curve 1) and simplified bilinear (curve 2)

Equation (24) is a simple bilinear expression able to offer a proper approximation of the nonlinear FE results, and useful for practical purposes. It is worth remembering that the results herein obtained are valid for masonry panels under double bending conditions, as this is the hypothesis implicitly assumed in Eq. (2).

6 Analyses of unreinforced masonry façades

The effects of the b shape factor are discussed through the analysis of the capacity curves and the damage patterns of three plane masonry walls with regular openings, which represent the typical façades of existing buildings. The capacity diagrams were evaluated through a pushover approach, and both equivalent frame models (EFM), built using the code SAM (Simplified Analysis Method) II (Magenes and Calvi 1996, 1997), and finite element models (FEM), built using the code ANSYS, were employed. According to the EFM approach each masonry wall is subdivided into piers and spandrels, modelled with one-dimensional macro-elements (which are connected by rigid nodes) and the whole masonry wall is analysed as a framed structure. The in-plane behaviour of the macro-elements, both piers and spandrels, is assumed as elastic-perfectly plastic, with shear resistance and ultimate displacement obtained according to the provisions of the Italian Seismic Code (NTC 2008; Circular 2009). In particular the ultimate shear resistance is evaluated as the minimum between the resistance values for bending and diagonal cracking

while the ultimate displacement is conventionally assumed as a percentage of the height of the macro-elements, considering the corresponding typology of collapse. Since the code SAM II is based on the EFM approach, it needs a limited number of degrees of freedom, and it is hence possible to analyse large regular masonry structures with a relatively reduced computational effort. The interested reader can refer to Magenes and Della Fontana (1998) and Bucchi et al. 2013 for specific details and additional illustrative case studies.

In the analyses performed with the code SAM II, the b shape factor of the masonry beams was evaluated according to both the Eq. (12), as requested in the Circular (2009), and the Eq. (20), as herein proposed.

6.1 Geometrical and mechanical characteristics of the walls

Each of the three plane masonry walls includes five stories. The walls have a width of 17.0 m, are 15.0 m high and have a thickness of 45 cm (Fig. 23). To have spandrels with different slenderness the openings in each wall differ in their dimensions, as follows:

- FT wall has short spandrels. The slenderness of the spandrels in the three intermediate stories is $\lambda = l/h = 0.75$ (being l the span and h the height of the masonry beams). The average slenderness of all the spandrels is 0.883, the average slenderness of all the masonry piers is 1.086.
- FM wall has spandrels higher than the FT wall: the slenderness of the spandrels in the three intermediate stories is $\lambda = 1.0$. The average slenderness of all the spandrels is 1.150, the average slenderness of all the masonry piers is 1.314.
- FS wall has slender spandrels. The slenderness of the spandrels in the three intermediate stories is $\lambda = 2.0$. The average slenderness of all the spandrels is 2.0, the average slenderness of all the masonry piers is 1.657.

The masonry walls were assumed not reinforced; only a concrete lintel well connected to the surrounding masonry was supposed over each opening (as usual in this building typology). The masonry mechanical parameters are the same assumed in Sect. 4.2, i.e.: longitudinal modulus of elasticity $E = 2000$ N/mm^2, shear modulus of elasticity $G = 800$ N/mm^2, compressive strength $f_m = f_{cDP} = 1.522$ N/mm^2, tensile strength $f_t = f_{tWW} = 0.15$ N/mm^2, shear strength $\tau_0 = f_t/1.5 = 0.1$ N/mm^2 and, compressive strength in the horizontal direction $f_h = f_m = 1.522$ N/mm^2. They correspond to a masonry made of bricks and aerial lime mortar with poor mechanical characteristics, according to the bounds reported in the Circular (2009).

The walls were subjected to their own weight (specific weight $w = 18.0$ kN/m^3) and to the vertical loads of the floors, supposed to be equal to 10 kN/m.

6.2 Masonry walls modelling and collapse modes for the EF models

The masonry walls were modelled with both the FEM technique and the EFM approach.

The FE models were built using 8-node three-dimensional isoparametric finite elements (*Solid 65*) with size 0.2 × 0.2 × 0.2 m (Fig. 24 shows the discretization of the FT wall). The mechanical nonlinear masonry behaviour was still reproduced by combining the Drucker–Prager plasticity surface (Drucker and Prager 1952) with the Willam–Warnke failure criterion (Willam and Warnke 1975), and the constitutive parameters are reported in Table 4. Concrete lintels were modelled by using the same mechanical models, with modified parameters to account for a concrete of resistance class C25/30.

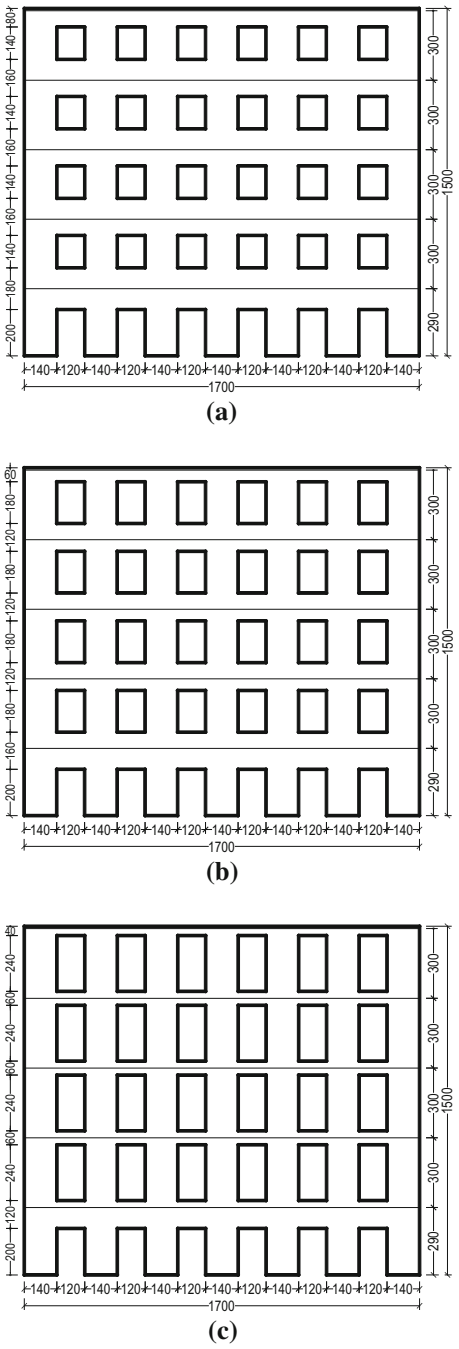

Fig. 23 Geometry of the three plane masonry walls: **a** FT; **b** FM; **c** FS (measures are in cm)

The code SAM II was employed to build the EF models. According to this approach each masonry wall is schematised with a system of deformable beams (reproducing masonry piers and spandrels) connected by rigid links (Fig. 25, wall FT). Vertical loads are

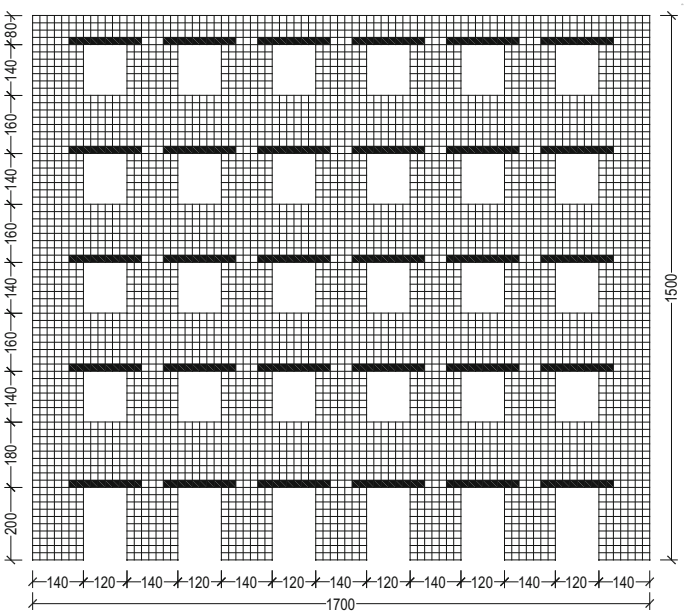

Fig. 24 FE model of FT wall (measures are in cm)

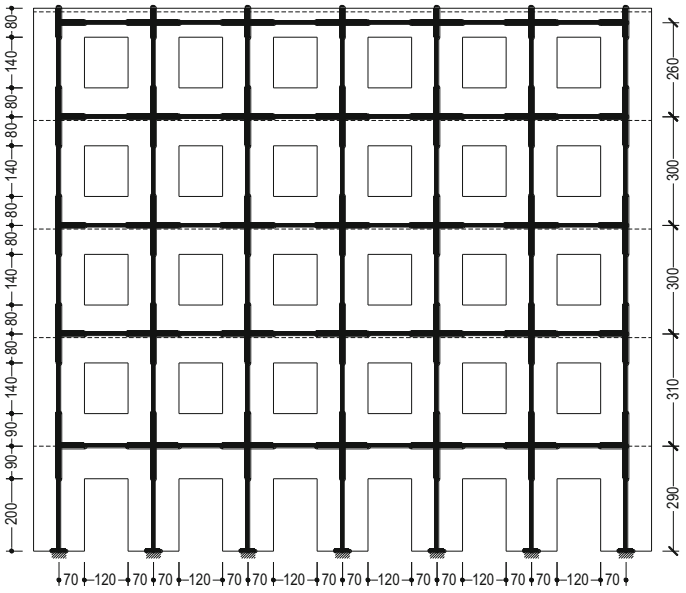

Fig. 25 EF model of FT wall (measures are in cm)

applied to the joints of the model at floor levels; horizontal seismic forces are applied to the centres of mass of each floor. The joints at the same level have the same horizontal displacement, therefore the assumption of rigid floor diaphragms holds. The mechanical properties required by SAM II are reported in Table 7.

Table 7 Mechanical properties of the masonry (EFM analyses)

Elastic parameters		
E	Longitudinal modulus of elasticity	2000 N/mm^2
G	Shear modulus of elasticity	800 N/mm^2
w	Weight per unit volume	18.0 kN/m^3
Masonry strenght and collapse parameters		
μ	Friction coefficient	0.4
f_m	Vertical compressive strength	1.522 N/mm^2
f_h	Horizontal compressive strength	1.522 N/mm^2
f_t	Diagonal shear strength	0.15 N/mm^2
f_{v0}	Pure shear strength	0.10 N/mm^2
d_p	Flexural drift	0.006
d_v	Shear drift	0.004
FC	Confidence factors	1.0

According to the NTC (2008) three failure modes were considered for masonry piers: bending, shear sliding and shear diagonal cracking (as discussed in Sect. 2). For instance, in case of diagonal cracking shear collapse, Eq. (2) was considered where f_{v0} corresponds to τ_0 and the values of the b shape factor were assumed according to the curve (2) of Fig. 6. The mechanical behaviour adopted for the masonry piers is elastic-perfectly plastic until they reach the limit values of the chord rotation. The shear drift limit d_v and the bending drift limit d_p are reported in Table 7.

For the spandrels, bending [Eq. (6)] and shear diagonal cracking failure [Eq. (2)] modes were considered. In the latter case, the values of the b shape factor in Eq. (2) were evaluated according to both Eq. (12) (as requested in the Circular 2009) and Eq. (20). The mechanical behaviour of the masonry spandrels, as assumed for the piers, is elastic-perfectly plastic until they reach the drift limits.

All the safety factors were assumed unitary, thus differences among the capacity curves are to be sought only in the different choice of the b shape factor.

6.3 Results of the pushover analyses

According to the pushover approach the horizontal forces were monotonically increased until collapse, and the displacement of a control point at the top level of each wall was recorded to build the capacity curves. The following distributions of the horizontal forces were considered (NTC 2008):

- triangular distribution (TD), i.e. horizontal forces proportional to the product of the masses times their height (measured from the base of the structure);
- modal distribution (MD), i.e. horizontal forces proportional to the product of the masses for the components of the in-plane modal shape;
- uniform distribution (UD), i.e. horizontal forces proportional to the mass distribution.

Figure 26 shows the capacity curves of the three walls for the distributions TD and UD for the three models: FEM, SAM II-A [EF models where b is evaluated according to Eq. (12)] and SAM II-B [EF models where b is evaluated according to Eq. (20)]. The results obtained with the modal distribution (MD) are very similar to those obtained with the triangular distribution (TD) and are not reported for brevity's sake. The capacity curves report the base shear V_b against the horizontal displacement d_c of the control point.

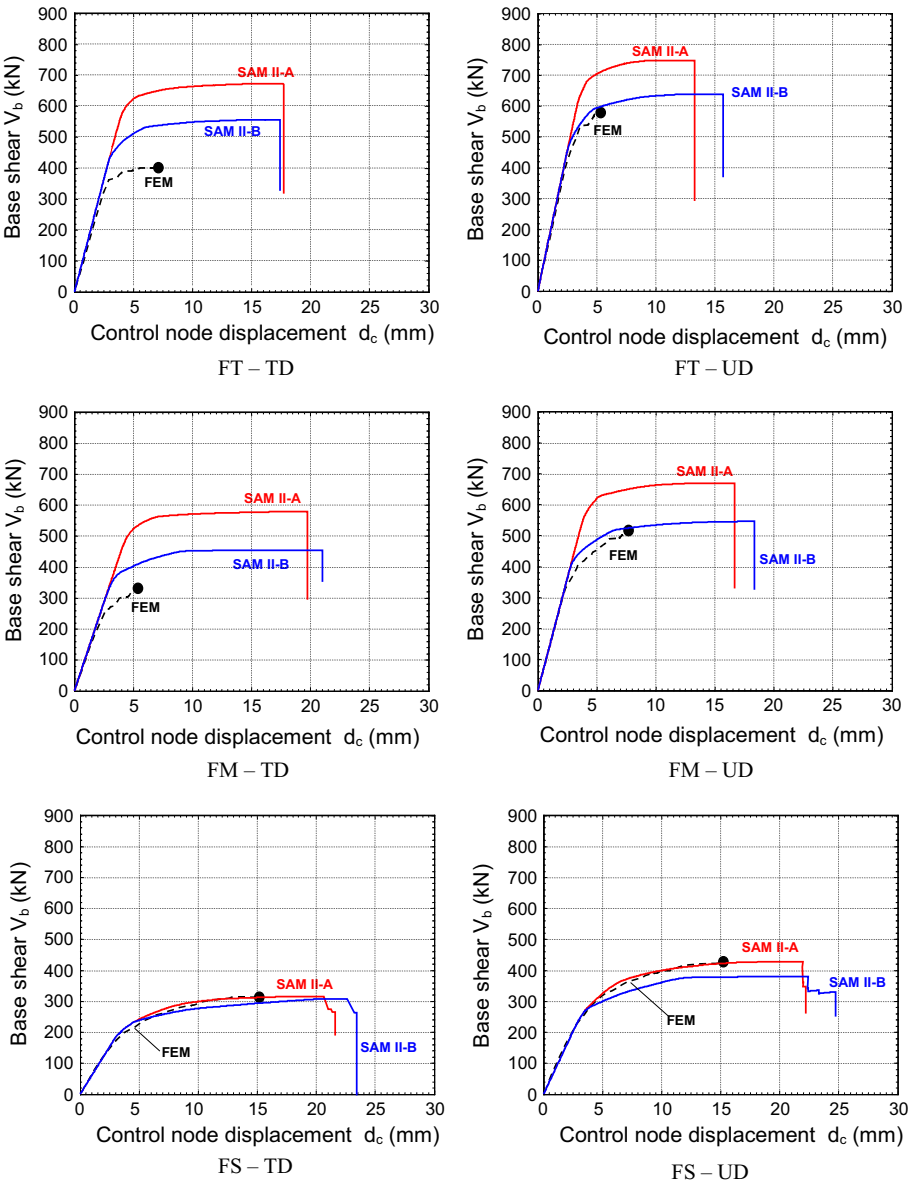

Fig. 26 Capacity curves obtained with triangular (TD) and uniform (UD) distributions. FEM = finite element model; SAM II-A = equivalent frame model with b evaluated according to NTC (2008); SAM II-B = equivalent frame model with b evaluated according to Eq. (20)

Following quantities were analysed: the initial stiffness K_e, the maximum base shear V_{bu} and the maximum displacement of the control point d_{cu}. These results are summarised in Tables 8, 9 and 10.

In terms of initial stiffness K_e there is a substantial agreement between the FE and EF models, with differences ranging between −13 and +10 %.

Table 8 FT wall: comparison between FEM and EFM pushover results

Load distribution	K_e/K_{eFEM}			V_{bu}/V_{buFEM}			d_{cu}/d_{cuFEM}		
	FEM	SAM II-A	SAM II-B	FEM	SAM II-A	SAM II-B	FEM	SAM II-A	SAM II-B
TD	1.00	1.10	1.10	1.00	1.68	1.38	1.00	2.45	2.41
MD	1.00	1.09	1.09	1.00	1.63	1.35	1.00	2.35	2.36
UD	1.00	1.05	1.05	1.00	1.29	1.10	1.00	2.46	2.90

Table 9 FM wall: comparison between FEM and EFM pushover results

Load distribution	K_e/K_{eFEM}			V_{bu}/V_{buFEM}			d_{cu}/d_{cuFEM}		
	FEM	SAM II-A	SAM II-B	FEM	SAM II-A	SAM II-B	FEM	SAM II-A	SAM II-B
TD	1.00	1.05	1.05	1.00	1.73	1.36	1.00	3.68	3.92
MD	1.00	1.03	1.03	1.00	1.51	1.19	1.00	2.25	2.47
UD	1.00	1.00	1.00	1.00	1.28	1.05	1.00	2.13	2.34

Table 10 FS wall: comparison between FEM and EFM pushover results

Load distribution	K_e/K_{eFEM}			V_{bu}/V_{buFEM}			d_{cu}/d_{cuFEM}		
	FEM	SAM II-A	SAM II-B	FEM	SAM II-A	SAM II-B	FEM	SAM II-A	SAM II-B
TD	1.00	0.90	0.90	1.00	1.00	0.98	1.00	1.41	1.53
MD	1.00	0.87	0.87	1.00	0.94	0.93	1.00	0.99	1.06
UD	1.00	0.87	0.87	1.00	1.00	0.89	1.00	1.44	1.61

More interesting are the comparisons about the maximum base shear V_{bu} because the b shape factor directly affects the shear strength of the spandrels: if the b values are underestimated the shear strength is overestimated, causing an increase of V_{bu}. The capacity curves obtained with the FE models, which do not depend on factor b, are used as reference to check the effectiveness of the results obtained with the EF models. A first examination of the results shows that the EF models of FT and FM walls develop base shear V_{bu} greater than those obtained with the FE approach. These differences tend to decrease along with the uniform distribution; on the contrary a good agreement for all load distributions is obtained for the FS wall. In detail, the SAM II-A models of FT and FM walls for load distributions TD and MD, provide V_{bu} values exceeding 1.5 times those obtained with the FE models (the maximum difference is about 70 %, which decreases to about 28 % in the case of uniform load distribution UD). These differences appreciably decrease with the SAM II-B models [where b is evaluated according to Eq. (20)]. The maximum difference becomes about 38 % (FT wall with the triangular distribution TD), the minimum is about 5 % (FM wall with the uniform distribution UD). The response of the FS wall is slightly different from the other two. In almost all the analyses (TD, MD, UD) the EF models offer values of V_{bu} lower than those obtained with the FE models.

Furthermore, the V_{bu} evaluated with the SAM II-B models are greater than those obtained with the SAM II-A models.

Concerning the displacements, in case of FT and FM walls the EF models offer displacements that differ of about +292 % from those obtained with the FEM (reduced to about 53 % in case of the FS wall). These discrepancies do not depend on the formulation adopted for the *b* shape factor, but are instead a consequence of the different solution algorithm adopted by the FE and the EF codes. The FE software performs a control force analysis, hence it is only able to reproduce the initial branch of the pushover curve, but not the descending one. Therefore the displacements obtained with the FEM are those corresponding to the maximum base shear. Save for this point, the results of the EFM of FT and FM walls are in good agreement with the one obtained with the FEM when the *b* shape factor is evaluated according to Eq. (20).

6.4 Analysis of the damage in the masonry walls

Figures 27, 28 and 29 show, for FT, FM and FS walls respectively, the damage maps obtained at the end of each analysis (distributions TD and UD; the results obtained with the distribution MD are similar to those obtained with TD and are not reported for brevity's sake).

For the FE models, according to the assumption of the smeared crack, the damage is shown as cracking and crushing distribution on the façade. For the EFM the damage of piers or spandrels (symbolised at the end or in the middle section of each element) is represented as follows: (●) denotes bending failure, (×) denotes shear failure with diagonal cracking and (♦) denotes shear sliding failure (only for masonry piers).

For the FS wall (Fig. 29) a good agreement between the damage maps obtained with the two codes is observed. For FT and FM walls (Figs. 27, 28) several differences arise. This can be interpreted as follows: in the FE models the cracks propagate and spread around the diagonals of the walls (with a more evident spread for FT wall, less for FM wall). This result is consistent: the shorter are the spandrels (the smaller are the openings), the more the behaviour of the wall is similar to that of a masonry panel under horizontal loads. Consequently, the principal tensile stresses take the direction of the diagonal of the panels, and cracking develops where the tensile strength is exceeded. This does not occur for the FS wall, where the damage affects first the thin spandrels and, subsequently, propagates to piers. In the EF models the behaviour is different since the assumption of rigid floor diaphragms allows for a global structural response of all resisting elements, ensuring a wider distribution of seismic forces between them. The FE models do not have rigid diaphragms, which explain the existing differences in these two walls (FT and FM). This is indirectly confirmed by the fact that the capacity curves of the FS wall present the best agreement. Furthermore, for all the walls the FE models show (regardless of the assumed distribution of horizontal forces) a sensible damage in some parts of the joints between piers and spandrels. This does not occur in the EF models where this area is assumed as infinitely stiff and strong.

Table 11 resumes the number of failures observed in each wall: M indicates the number of bending collapses, V_D denotes the number of diagonal cracking failures and V_S indicates the number of shear sliding collapses. None of the piers collapses for shear with diagonal cracking: they collapse only for bending or shear sliding. It is also evident that evaluating the *b* shape factor according to Eq. (20) originates an increase in the number of collapses for diagonal cracking and a reduction in the number of collapses for shear sliding. A clear change in the number of collapses for bending by varying the criterion for calculating the *b* shape factor is not observed. SAM II-B models showed increases of bending failure in 4 cases out of 9: two for the uniform distribution of FT and FM walls, two for the triangular

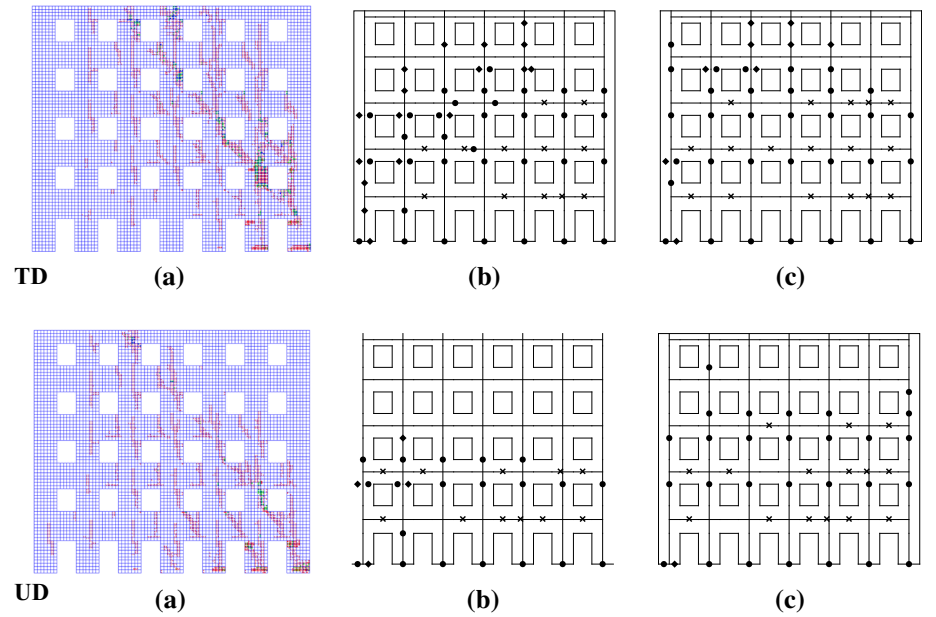

Fig. 27 Damage maps of FT wall under triangular (TD) and uniform (UD) load distributions: **a** FEM; **b** SAM II-A; **c** SAM II-B

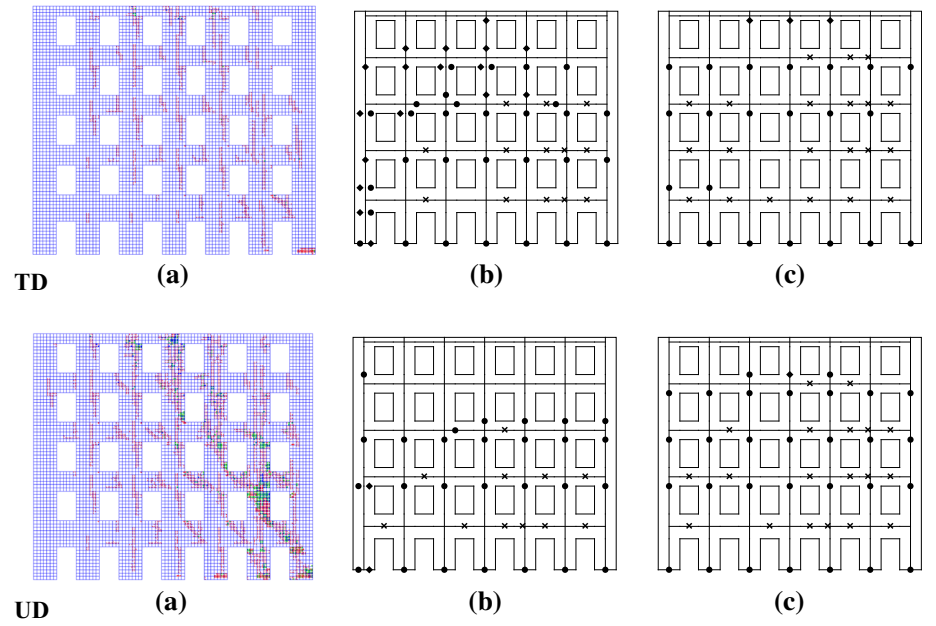

Fig. 28 Damage maps of FM wall under triangular (TD) and uniform (UD) load distributions: **a** FEM; **b** SAM II-A; **c** SAM II-B

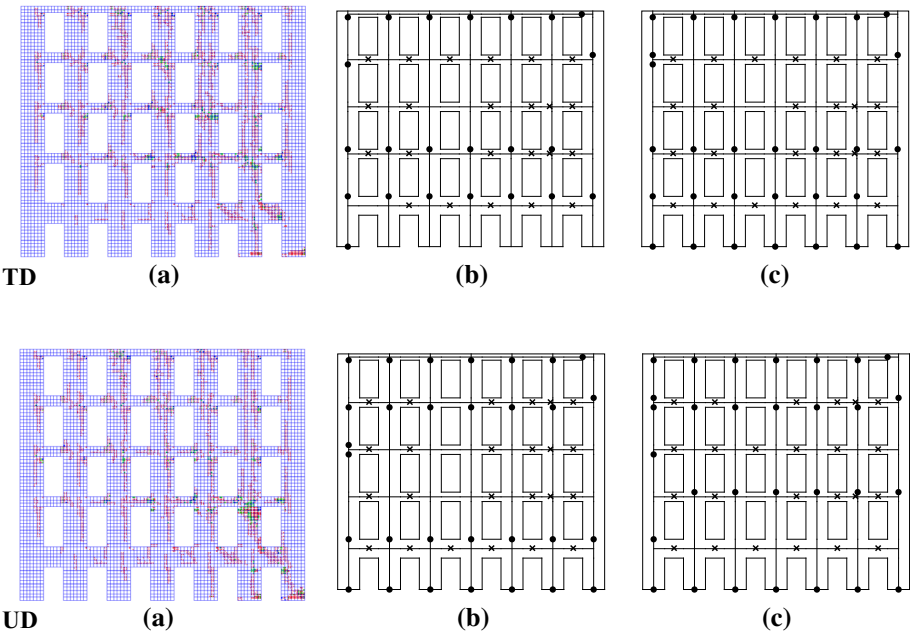

Fig. 29 Damage maps of FS wall under triangular (TD) and uniform (UD) load distributions: **a** FEM; **b** SAM II-A; **c** SAM II-B

Table 11 EF models: numbers and typologies of masonry panels failures

Wall	Load distribution	*b*—Eq. (12)			*b*—Eq. (20)		
		M	V_D	V_S	M	V_D	V_S
FT	TD	33	12	17	33	17	9
FT	MD	36	11	18	29	17	8
FT	UD	20	11	4	28	15	1
FM	TD	30	13	17	22	21	3
FM	MD	33	14	16	21	21	4
FM	UD	27	11	2	30	19	1
FS	TD	23	23	–	30	24	–
FS	MD	23	23	–	28	24	–
FS	UD	30	24	–	30	24	–

and the modal distributions of the FS wall. In the remaining cases the number of bending failures remains the same or decreases, with respect to the SAM II-A models.

7 Conclusive remarks

Results of this study suggest that the equation of the *b* shape factor adopted by the current Italian Seismic Code (NTC 2008) is affected by a significant approximation when it is applied to short masonry panels. The *b* values here evaluated by means of linear and nonlinear numerical analyses are higher than those obtained from the simplified

formulation adopted by the NTC (2008), resulting in a reduction in the shear strength of the masonry panels. An amendment for the b shape factor is then proposed according to the obtained numerical results. To assess the effects of the proposed amendment, the seismic capacity of three plane URM walls with different slenderness of the masonry beams were investigated through pushover analyses, focusing the attention on the b shape factor. The walls were modelled by both finite element and equivalent frame models, and in the latter case the b shape factor was assumed, for comparative purposes, according to both the NTC (2008) and the proposed amendment. The FEM results are independent from the b coefficient and were used as reference. Results of the investigations in terms of elastic stiffness K_e show a good agreement in all the pushover analyses for all the walls. On the contrary, differences were observed for the ultimate base shear V_{bu}. The EF models of FT and FM walls produced higher values of V_{bu} with respect to the FE models results. This difference was amplified when the b factor was evaluated according to the NTC (2008). The obtained results thus highlighted a criticism of the actual Italian Seismic Code, and suggest the need for further researches on the subject by an experimental campaign. In this respect, it is proposed to adjust the formulation for b included in the NTC (2008) introducing the alternative relationship herein suggested.

References

ANSYS (1992) Revision 5.0 (user's manual, theory manual). Swanson Analysis System Inc., Houston

ASCE/SEI 41-06 (2006) Seismic rehabilitation of existing buildings. American Society of Civil Engineers, Reston

Augenti N (2004) Il calcolo sismico degli edifici in muratura. UTET, Torino (in Italian)

Benedetti D, Tomaževic M (1984) Sulla verifica sismica di costruzioni in muratura. Ing Sismica I(0):9–16 (in Italian)

Betti M, Vignoli A (2011) Numerical assessment of the static and seismic behaviour of the basilica of Santa Maria all'Impruneta (Italy). Constr Build Mater 25(12):4308–4324

Betti M, Galano L, Vignoli A (2009) Analisi sismica non lineare di pareti in muratura e confronti con la normativa. In: Atti del workshop on design for rehabilitation of masonry structures, wonder masonry 3, Ischia, Lacco Ameno, pp 514–525 (in Italian)

Betti M, Galano L, Vignoli A (2014) Comparative analysis on the seismic behaviour of unreinforced masonry buildings with flexible diaphragms. Eng Struct 61:195–208

Bucchi F, Arangio S, Bontempi F (2013) Seismic assessment of an historical masonry building using nonlinear static analysis. In: Proceedings of the fourteenth international conference on civil, structural and environmental engineering computing. Paper 72

Calderini C, Cattari S, Lagomarsino S (2009) In-plane strength of unreinforced masonry piers. Earthq Eng Struct Dyn 38(2):243–267

Chen SY, Moon FL, Yi T (2008) A macroelement for the nonlinear analysis of in-plane unreinforced masonry piers. Eng Struct 30(8):2242–2252

Chiostrini S, Vignoli A (1994) In-situ determination of the strength properties of masonry walls by destructive shear and compression tests. Mason Int 7(3):87–96

Chiostrini S, Galano L, Vignoli A (1998) In-situ tests and numerical simulations on structural behaviour of ancient masonry. In: Proceedings of the workshop on seismic performance of monuments. Lisbon, pp 197–206

Circular 1981 (1981) Istruzioni relative alla normativa tecnica per la riparazione ed il rafforzamento degli edifici in muratura danneggiati dal sisma, Circolare del Ministero dei Lavori Pubblici 30 Luglio 1981 n. 21745 (in Italian)

Circular 2009 (2009) Istruzioni per l'applicazione delle "Nuove norme tecniche per le costruzioni" di cui al D.M. del 14/01/2008, G.U. n. 47, 26 Febbraio 2009, S.O. n. 27. Circolare del Ministero delle Infrastrutture 2 Febbraio 2009, (in Italian)

DM 1996 (1996) Norme tecniche per le costruzioni in zone sismiche, D.M. del Ministero dei Lavori Pubblici 16 Gennaio 1996, G.U. n. 29, 5 Febbraio 1996, (e Circolare del Ministero LL. PP. 10 Aprile

1997, n. 65/AA.GG., Istruzioni per l'applicazione delle "Norme tecniche per le costruzioni in zone sismiche", di cui al D.M. LL. PP. 16 Gennaio 1996) (in Italian)
Drucker D, Prager W (1952) Soil mechanics and plastic analysis or limit design. Q Appl Math 10(2):157–165
EN 1996-1 (2005) Eurocode 6: design of masonry structures—part 1–1. General rules for reinforced and unreinforced masonry structures. CEN (European Committee for Standardization), Brussels
FEMA 306 (1998) Evaluation of earthquake damaged concrete and masonry wall buildings. Federal Emergency, Washington
FEMA 356 (2000) Prestandard and commentary for the seismic rehabilitation of buildings. Federal Emergency Management Agency, Applied Technology Council (ATC), Washington
Magenes G, Calvi GM (1996) Prospettive per la calibrazione di metodi semplificati per l'analisi sismica di pareti murarie. Atti del Convegno Nazionale "La Meccanica delle Murature tra Teoria e Progetto", Messina, pp 503–512 (in Italian)
Magenes G, Calvi GM (1997) In-plane seismic response of brick masonry walls. Earthq Eng Struct Dyn 26:1091–1112
Magenes G, Della Fontana S (1998) Simplified non-linear seismic analysis of masonry buildings. Proc Br Mason Soc 8:190–195
NTC 2008 (2008) Nuove Norme Tecniche per le Costruzioni, G.U. n. 29, 4 Febbraio 2008, S.O. n. 30. D.M. del Ministero delle Infrastrutture e dei Trasporti 14 Gennaio 2008 (in Italian)
Tomaževic M (1978) The computer program POR. Report ZRMK, Institute for Testing and Research in Materials and Structures, Ljubljana (in Slovenian)
Tomaževic M (2009) Shear resistance of masonry walls and Eurocode 6: shear versus tensile strength of masonry. Mater Struct 42:889–907
Tremayne B, Turner F, Russell A, Oliver S, Derakhshan H (2012) Proposed update to masonry provisions of ASCE/SEI 41: seismic evaluation and retrofit of existing buildings. In: Proceedings of the 15th world conference on earthquake engineering, Lisbon
Turnšek V, Cacovic F (1971) Some experimental results on the strength of brick masonry walls. In: Proceedings of the 2nd international brick masonry conference, stoke-on-trent, pp 149–156
Turnšek V, Sheppard P (1980) The shear and flexural resistance of masonry walls. In: Proceedings of the international research conference on earthquake engineering, Skopje, pp 517–573
Willam KJ, Warnke EP (1975) Constitutive model for the triaxial behaviour of concrete. In: Proc IASBE Sem Concr Struct Subj Triaxial Stress Bergamo, vol 19. pp 1–30
Zucchini A, Lourenço PB (2007) Mechanics of masonry in compression: results from a homogenisation approach. Comput Struct 85(3–4):193–204